Monthly Notices
of the
ROYAL ASTRONOMICAL SOCIETY

MNRAS **463,** 2242–2264 (2016)
Advance Access publication 2016 August 24

doi:10.1093/mnras/stw2130

On the formation of a quasi-stationary twisted disc after a tidal disruption event

M. Xiang-Gruess,[1,2]★ P. B. Ivanov[3] and J. C. B. Papaloizou[1]

[1]*DAMTP, Centre for Mathematical Sciences, University of Cambridge, Wilberforce Road, Cambridge CB3 0WA, UK*
[2]*Helmholtz-Institut für Strahlen- und Kernphysik, Nussallee 14-16, D-53115 Bonn, Germany*
[3]*Astro Space Centre, P. N. Lebedev Physical Institute, 4/32 Profsoyuznaya Street, Moscow 117810, Russia*

Accepted 2016 August 21. Received 2016 August 21; in original form 2016 June 11

ABSTRACT

We investigate misaligned accretion discs formed after tidal disruption events that occur when a star encounters a supermassive black hole. We employ the linear theory of warped accretion discs to find the shape of a disc for which the stream arising from the disrupted star provides a source of angular momentum that is misaligned with that of the black hole. For quasi-steady configurations, we find that when the warp diffusion or propagation time is large compared to the local mass accretion time and/or the natural disc alignment radius is small, misalignment is favoured. These results have been verified using smoothed particle hydrodynamics simulations. We also simulated 1D model discs including gas and radiation pressure. As accretion rates initially exceed the Eddington limit, the disc is initially advection dominated. Assuming the α model for the disc, where it can be thermally unstable, it subsequently undergoes cyclic transitions between high and low states. During these transitions, the aspect ratio varies from $\sim$1 to $\sim 10^{-3}$ which is reflected in changes in the degree of disc misalignment at the stream impact location. For maximal black hole rotation and sufficiently large values of viscosity parameter $\alpha > \sim$0.01–0.1, the ratio of the disc inclination to that of the initial stellar orbit is estimated to be 0.1–0.2 in the advection-dominated state, while reaching of order unity in the low state. Misalignment decreases with decrease of α, but increases as the black hole rotation parameter decreases. Thus, it is always significant when the latter is small.

Key words: accretion, accretion discs – hydrodynamics – relativistic processes – quasars: supermassive black holes.

1 INTRODUCTION

A tidal disruption event (TDE) occurs when a star approaches sufficiently close to a supermassive black hole that it is ripped apart by tidal forces. Its orbit must take it within the so-called tidal disruption radius, $R_{\rm T}$. This radius is such that the mean density of a mass equal to that of the black hole, assumed to be enclosed within a sphere of radius, $R_{\rm T}$, is equal to that of the star. The ensuing tidal disruption results in an accretion disc around black hole being formed from the stellar gas. This in turn gives rise to a luminous source of radiation.

Over the past two decades or so, around 30 candidate TDEs, where stars are tidally torn apart by supermassive black holes, have been identified, see e.g. Komossa (2015) for a review and further discussion. Normally, these are associated with non-stationary flares of soft X-ray radiation in the centres of previously non-active galaxies (e.g. Esquej et al. 2008). They are observed to decay on a timescale of the order of several years. Some manifest themselves as sources of transient optical line emission thought to originate from interstellar gas that has been ionized by X-ray radiation coming from a TDE (e.g. Komossa et al. 2008, 2009). Additionally, there are non-stationary powerful bursts of radiation over a very wide waveband, ranging from radio to X-rays, which are interpreted as being produced by processes occurring in a jet directed almost parallel to the line of sight. This is assumed to be formed during an early stage of the evolution of the accretion disc formed after a TDE. A canonical example of such an event is Swift J1644+57 (see Burrows et al. 2011).

TDEs provide an excellent opportunity to determine black hole parameters, study the physics of accretion and jet formation as well as investigate the nature of stellar populations in galactic centres. Theoretical investigations of TDEs were initiated approximately 40 years ago following a seminal paper of Hills (1975). Subsequently, many researches have considered aspects of the formation of TDEs, their properties and observational appearance. These studies can be characterized by allocating them to one of four interrelated groups.

The first of these is devoted to stellar dynamical processes occurring in the vicinity of single or binary supermassive black holes which result in the formation of stellar orbits with their

★ E-mail: mxiang@uni-bonn.de

periastrons close enough to the black hole for the stars on them to be tidally disrupted. Tidal disruption rates were evaluated for different parameters characterizing the central star clusters and black holes (see e.g. Frank & Rees 1976; Lightman & Shapiro 1977; Magorrian & Tremaine 1999; Syer & Ulmer 1999; Ivanov, Polnarev & Saha 2005; Stone & Metzger 2016). The second group focuses on the process of tidal disruption itself under different assumptions concerning the structure of the star, its orbit and the gravitational field of the black hole (e.g. Carter & Luminet 1983, 1985; Evans & Kochanek 1989; Khokhlov, Novikov & Pethick 1993a,b; Ivanov & Novikov 2001; Ivanov, Chernyakova & Novikov 2003; Ivanov & Chernyakova 2006; MacLeod, Guillochon & Ramirez-Ruiz 2012; Guillochon & Ramirez-Ruiz 2013; Dremova, Dremov & Tutukov 2014; Mainetti et al. 2016). The third group studies the formation, properties and dynamics of the accretion disc formed after a TDE (e.g. Cannizzo, Lee & Goodman 1990; Kochanek 1994; Kim, Park & Lee 1999; Stone & Loeb 2012; Hayasaki, Stone & Loeb 2013; Kelley, Tchekhovskoy & Narayan 2014; Shen & Matzner 2014; Franchini, Lodato & Facchini 2015; Guillochon & Ramirez-Ruiz 2015; Bonnerot et al. 2016; Coughlin et al. 2016). The fourth group explores the observational consequences of TDEs (e.g. Bogdanovic et al. 2004; van Velzen et al. 2011; Khabibullin et al. 2014; Miller 2015; Zhang et al. 2015).

It was pointed out by Lacy, Townes & Hollenbach (1982) with further development by Rees (1988) that when the stellar orbit is assumed to be parabolic and tidal forces totally disrupt the star, approximately one half of the stellar material gains positive orbital energy and is expelled from the system, while the remainder attains negative energy (or equivalently positive binding energy) and, accordingly, becomes gravitationally bound to the black hole. This can be seen if we adopt a simplified view of tidal disruption as occurring in an abrupt manner when the star reaches periastron. At that point, one half of the stellar material is situated closer to the black hole relative to the centre of mass of the star, while the remainder is further away. As the centre of mass follows an orbit with zero binding energy, the stellar material located deeper in the potential well of the black hole that is moving with the same velocity at the point of disruption will have a binding energy per unit mass equal to the difference between its potential energy per unit mass and the potential energy per unit mass at the centre of mass of the star. The corresponding discussion for material further away than the centre of mass implies that this will become unbound.

Gas elements comprising the bound material will in general have binding energies ranging between some largest absolute value and zero. Assuming that their subsequent motion is ballistic, their corresponding orbital periods will be in the range $P_{\rm min} < P_{\rm orb} < \infty$, where $P_{\rm min}$ corresponds to the orbital period of the most strongly bound material. Accordingly, they return to periastron at different times after the TDE forming a stream of gas that first arrives at periastron when a time, $\sim P_{\rm min}$, has elapsed after the star was tidally disrupted (e.g. Rees 1988). Supposing that the amount of mass occupying any small binding energy interval of a fixed extent is approximately uniform, it is easy to estimate that mass flux from this stream should be $\propto t^{-5/3}$ when $t \gg P_{\rm min}$ (e.g. Lodato, King & Pringle 2009, and references therein). At times of the order of $P_{\rm min}$, the stream starts to intersect itself near periastron as a result of e.g. Einstein precession, giving rise to the formation of strong shocks. These shocks convert stream kinetic energy into heat, which is later radiated away.

On the other hand, at a sufficiently early stage of the process, when friction arising from any effective viscosity will not have had enough time to produce significant effects, its specific angular momentum remains approximately equal to that of the initial stellar orbit. Thus, there is a tendency to form a gaseous torus with this specific angular momentum in the vicinity of the black hole (e.g. Cannizzo et al. 1990). On longer time-scales, action of an effective viscosity can cause the torus to spread, leading to the formation of an accretion disc (e.g. Lynden-Bell & Pringle 1974). Initially, estimates of the accretion rate from the stream indicate that it will be strongly super-Eddington. The disc is expected to be optically thick, radiation pressure dominated, and, possibly, associated with strong outflows.

When the black hole is non-rotating, the mid-plane of the accretion disc will coincide with that of the initial stellar orbit. However, in the case of a Kerr black hole, the Lense–Thirring force acts to drag it to coincide with the black hole equatorial plane (see e.g. Franchini et al. 2015, and references therein). On the other hand, the stream orbital plane is the same as that of the initial stellar orbit. This is in general expected to be inclined with respect to the black hole equatorial plane with an inclination angle order of unity. Accordingly, the stream material arriving in the region close to the initial periastron, after accretion disc formation and assumed relaxation to the equatorial plane, will impact the disc obliquely, pushing it out of the black hole equatorial plane. Thus, there is a possibility that the disc is inclined with respect to the black hole equatorial plane at radii of the order of the stream impact radius. This is expected even in the presence of precession of the stream orbit through some angle produced by black hole rotation; the magnitude of this angle is a function of the stellar orbital parameters, the black hole rotation parameter and time.

In addition, the combined action of black hole rotation and oblique stream impact leads to a non-trivial dependence of the disc tilt and twist angle on the distance from black hole. That the accretion disc is twisted could have a profound effect on its observational properties (see e.g. Bachev 1999; Caproni et al. 2007; Wu, Chen & Yuan 2010; Dexter & Fragile 2013). This could potentially be used as a diagnostic for the determination of the black hole mass and angular momentum as well as to probe the physical conditions in the accretion flow.

It is the purpose of this paper to determine the conditions under which the inclination angle at the stream impact radius can be large as well as to investigate the properties of twisted accretion discs formed after TDE. We tackle the problem using a combination of analytic and numerical techniques. First, we adapt the linear theory of twisted accretion discs (see e.g. Papaloizou & Pringle 1983; Papaloizou & Lin 1995). This formally assumes that the local inclination angle between the orbital plane of an annulus of orbiting disc material and the black hole equatorial plane is small throughout the disc.[1] In this theory, the disc tilt and twist are treated as perturbations on a flat disc (background) model. We suppose that the relaxation time for the disc to attain a quasi-steady twisted tilted configuration is smaller than a time-scale characterizing the evolution of the background flat disc. As the propagation time for either bending waves or warp diffusion is in general expected to be short compared to the disc evolution time on account of mass redistribution (see Papaloizou & Pringle 1983; Papaloizou & Lin 1995), for the most part this is expected to be reasonable. Accordingly,

[1] In a situation where the inclination angle at the stream impact radius is of the order of the inclination of the stellar orbit, as we have indicated, it is in general expected to be large. However, we believe that our assumption that it is small does not affect estimates of the conditions under which this angle will be significant.

we limit consideration to such quasi-stationary configurations. We derive an equation governing the tilt and twist of the disc for which the stream provides a torque through a source term acting at the stream impact location. The magnitude of the torque is determined by the magnitude of the inflowing angular momentum components perpendicular to the black hole rotation axis which arise on account of obliquity of the orbital plane of the stream.

We use the governing equation to determine the parameters of the problem that are important for indicating when there will be significant misalignment between the disc mid-plane and the black hole equatorial plane. These are found to be a quantity measuring the ratio of the warp diffusion or propagation time to the local mass accretion time, together with the ratio of the alignment radius to the stream impact radius. For radii smaller than the alignment radius, the disc mid-plane is significantly modified by the black hole in the absence of the stream. The dependence on these parameters is investigated using numerical solutions of the governing equation as well as an asymptotic analytic approach. In particular, we find that large values of the first parameter and small values of the second favour misalignment.

We test the above approach by performing three-dimensional numerical simulations using an appropriately modified smoothed particle hydrodynamics (SPH) code GADGET-2. These simulations follow the development of a twisted tilted disc sourced by a stream produced from tidally disrupted stellar material with the expected range of orbital binding energies. We find that the approaches obtain the same dependence of misalignment on the black hole rotation parameter with a typical difference between disc inclination angles at the stream impact radius, estimated from the analytic approach, and those obtained from the numerical simulations, after an initial relaxation period, of about 30 per cent, even when the angles are not small, thus validating our general approach.

We go on to study the longer term evolution of the background disc taking account of both gas and radiation pressure using a one-dimensional numerical scheme based on the finite difference code NIRVANA. This is a practical approach given the large dynamic range in this problem coupled with the need to consider evolution times greatly exceeding the shorter dynamical time-scales present in the system. It is approximate in that a vertical average is performed even though the disc is thick at an early stage when thermal instability leads to the disc being in a high advection-dominated state (see also the slim disc modelling of Abramowicz et al. 1988). We determine the evolution of the background accretion disc model, incorporating a mass supply from the stream, through the advection-dominated super-Eddington stage until the beginning of the standard thin disc radiative stage, for different values of the Shakura–Sunyaev viscosity parameter α. In the course of this evolution, the disc semi-thickness, H, experiences a very dramatic change from being of the order of the radial scale, R, during the advection-dominated stage down to values of the order of $10^{-3}R$ at the radiative stage, which has an important consequence for the evolution of the inclination angle.

This transition happens when a typical accretion rate through the disc at scales of interest is of the order of a few Eddington accretion rates.[2] It occurs in an unsteady manner with parts of the disc alternating between high and low states as the accretion rate due to the stream slowly declines. In this context, we note that in the standard Shakura–Sunyaev model for which the vertically integrated viscous stress is proportional to the vertically integrated sum of the radiation and gas pressures with the constant of proportionality being α, a thermal instability operates when the radiation pressure is larger than that of gas (see e.g. Shakura & Sunyaev 1976). This results in a limit cycle-like behaviour at various locations in the disc after the transition to the radiative phase begins. The transitions are found to occur at progressively smaller radii as the accretion rate into the disc decreases. During such transitions, the disc aspect ratio $\delta = H/R$ experiences a set of transitions between 'low' $\delta \sim 10^{-3}$ and 'high' $\delta \sim 1$ values until the total pressure in the disc drops down to values such that it becomes dominated by that of gas (see e.g. Szuszkiewicz & Miller 1997, 1998, 2001).

Under our assumption that the disc inclination relaxation time is short compared to the background disc evolution time when it undergoes such cycles, we will see that the cyclic behaviour is reflected in similarly sharp changes of the disc inclination angle at the stream impact radius between relatively large values at a low state and smaller values during a high state. We use numerical models of the background disc obtained from the 1D evolution studies as background models for the quasi-stationary equation describing the disc twist and tilt introduced above, and use this to calculate the evolution of disc inclination through the advection-dominated stage until the transition to the radiative stage.[3]

We show that when $\alpha > \sim 0.1$ and black hole rotation is close to maximal, typical inclination angles of the disc are of the order of $\sim$0.1–0.2 of the stream inclination angle at the advection-dominated stage.[4] However, the inclination angle becomes larger as the disc aspect ratio decreases, even in high states, at later times. In addition, the inclination can grow to values close to that of the stream during transitions to low states. Furthermore, disc inclinations get larger for smaller black hole rotations at all stages of the evolution of the disc.

The plan of the paper is as follows. In Section 2, we introduce basic quantities and associated space and time-scales used below. In Sections 3–3.2 we discuss the equation governing the disc tilt and twist as well as its solution for a model case with constant aspect ratio, δ. Section 4 is devoted to SPH modelling of the problem on hand and the comparison between the semi-analytic and SPH approaches. In Section 5, we describe the 1D grid-based simulations and go on to describe the evolution of the background aligned disc models. We go on to discuss solutions to our equation governing the disc inclination which incorporates models obtained from the 1D simulations as background models in Section 5.8. In Section 6, we provide analytic estimates of the disc inclination during the low state for values of the viscosity parameter smaller than those adopted for our numerical work. These are based on an asymptotic analytic theory of solutions of the equation governing disc tilt and twist developed in Appendix A. Finally, in Section 7, we discuss our results and set down our conclusions.

[2] We define the Eddington accretion rate, $\dot{M}_{\rm E}$, as the Eddington luminosity divided by square of speed of light c: for pure hydrogen $\dot{M}_{\rm E} = \frac{4\pi G m_{\rm p} M}{c\sigma_{\rm T}}$, where G is the gravitational constant, $m_{\rm p}$ and M are the proton mass and black hole mass, respectively, and $\sigma_{\rm T}$ is the Thomson cross-section.

[3] Note that, strictly speaking as we assumed the disc to be thin, our twist equation should be modified when the advection-dominated stage is considered. However, again we assume that this equation can be used during this stage to obtain approximate estimates. In particular, the result that the inclination is relatively small then is unlikely to be affected as this is a consequence of the relatively short accretion time in comparison to the warp diffusion time. A more accurate treatment of the problem will be considered elsewhere.

[4] At smaller values of α, the angles are estimated to be even smaller during this stage.

Table 1. Table of parameters, variables and symbols.

Symbol	Definition
R, $R_{\rm in}$, $R_{\rm out}$, R_*, $R_{\rm S}$	Radius, disc inner radius, disc outer radius, stellar radius and radius to stream impact location
$R_{\rm p}$, $R_{\rm T}$, $R_{\rm g}$, $R_{\rm BP}$, $R_{\rm rel}$	Periastron radius, tidal radius, gravitational radius, and, alignment scales for large and small viscosity
η, $\eta_{\rm rel}$	These are defined by $\eta = R_{\rm BP}/R_{\rm S}$ and $\eta_{\rm rel} = R_{\rm rel}/R_{\rm S}$
$B_{\rm S}$, $B_{\rm p}$	Penetration factors for stream and periastron
r, ϵ, $r_{\rm in}$, $r_{\rm out}$, $r_{\rm p}$	Dimensionless radius, softening parameter, and inner and outer boundary radii, and $r_{\rm p} = R/R_{\rm p}$
β, $\beta_{\rm S}$, β_*	Inclinations with respect to the black hole equatorial plane of the disc, the disc at the stream impact and the stream
M, M_6, $M_{\rm D}$	Black hole mass, black hole mass in units of 10^6 solar masses and disc mass
$\dot{M}$, $\dot{M}_{\rm S}$, $\dot{M}_{\rm E}$	Mass accretion rate, mass accretion rate from stream and mass accretion rate at Eddington limit
m, $m_{\rm p}$, $\dot{m}$, κ	Stellar mass, proton mass, dimensionless accretion rate and opacity
(X, Y, Z)	Cartesian coordinates with (X, Y) plane coinciding with the black hole equatorial plane
(X', Y', Z'), (R, θ, ϕ)	Cartesian and spherical polar coordinates with (X', Y') plane containing the stream
δ, H, Δ, δ_Δ	Aspect ratio, disc semi-thickness, relative radial width of stream input and nascent δ function
t, t_*, $\Omega_{\rm S} \equiv t_{\rm S}^{-1}$, $\Omega_{\rm p}^{-1} \equiv t_{\rm p}$	Time, characteristic dynamical time of star, orbital angular frequencies at the stream impact location and at periastron
$\mathcal{W}$, $\mathcal{W}_*$, $\mathcal{W}_+$, $\mathcal{W}_-$	Complex inclination $\beta e^{{\rm i}\gamma}$ of the disc in general, at the stream location, and for outer and inner solutions
Σ, Σ_0	General and characteristic surface densities. Note that the dimensionless quantity $\tilde{\Sigma} = \Sigma/\Sigma_0$
Σ_1, $\Sigma_{\rm high}$	Scaling parameter for disc surface density and high state value. Note that $\tilde{\Sigma}_{\rm high} = \Sigma_{\rm high}/\Sigma_0$
$k = 3GM/(c^2\alpha R)$	Parameter measuring the importance of post-Newtonian effects relative to viscosity
$\xi = \Sigma\delta^2 R^{1/2}$	Parameter proportional to viscous mass flux in outer disc
σ, $\sigma_{\rm max}$, $\sigma_{\rm rel,\,max}$	Parameter measuring the ratio of time-scales for warp diffusion and local mass accretion, and estimates for this and $\sigma_{\rm rel} = k\sigma$ in the high state
$\boldsymbol{J}$, $J_{\rm S}$	Black hole angular momentum($J = \|\boldsymbol{J}\|$) and specific angular momentum of stream
$\boldsymbol{L} = (L_X, L_Y, L_Z)$, T_X, T_Y	Disc angular momentum vector and torque components
$\dot{\mathcal{L}} = \sqrt{GMR_{\rm S}}\dot{M}_{\rm S}\lambda\mathcal{W}_*$	Rate of input of angular momentum due to stream with $\lambda = \sqrt{2R_{\rm p}/R_{\rm S}}$ normally equal to unity
ν, α, $\alpha_{\rm crit}$, α_{-2}	Kinematic viscosity, viscosity parameter, critical value of α below which relativistic effects matter and 100α
$P_{\rm min}$, P, $P_{\rm r}$, T, $\mathcal{R}$, μ	Minimum period, pressure, radiation pressure, temperature, gas constant and mean molecular weight
Φ, G, c, $\boldsymbol{F}_{\rm GM}$, Ψ,	Gravitational potential, gravitational constant, speed of light, gravitomagnetic force per unit mass and phase
a, a_R, $\sigma_{\rm T}$	Black hole rotation parameter, Stefan–Boltzmann constant and Thompson cross-section
$\Omega_{\rm LT}$, $L_{\rm E}$	Lense–Thirring frequency and Eddington luminosity
$\hat{\boldsymbol{l}}$, $\hat{\boldsymbol{l}}_*$, $\hat{\boldsymbol{k}}$	Unit vector in the direction of the disc angular momentum, at the stream location, and in the Z direction
$\boldsymbol{v}$, $\boldsymbol{R}$, $\boldsymbol{v}_\perp = \boldsymbol{\omega} \times \boldsymbol{R}$, $\boldsymbol{a}$, $\boldsymbol{f}_v$	Velocity, position vector, velocity component perpendicular to $\boldsymbol{R}$, acceleration and viscous force per unit area
$v_{\rm R}$, $c_{\rm s}$, U, ρ, $\langle\rho\rangle$	Velocity in radial direction, sound speed, internal energy density, density and projected density
ϵ_v, E, Π	The rate of energy input per unit area, and vertically integrated internal energy density and pressure
$t_{\rm sound}$, $t_{\rm TH}$, $t_{\rm TW}$	Characteristic sound crossing time, thermal time and warp diffusion time at stream impact location
τ, $\tau_{\rm crit}$	Time in units of $P_{\rm min}$ and value of τ at first high state-to-low state transition (time $= t_{\rm crit}$)

2 BASIC DEFINITIONS AND NOTATION

We investigate the influence of the gas stream produced as a result of a TDE on the form and structure of an accretion disc around a rotating black hole using both analytic and numerical methods. We envisage the situation where the entire accretion disc is formed from the gas stream resulting from the TDE. At any stage, the stream interacts with a disc produced as a result of the circularization and subsequent viscous spreading of stream material that arrived previously. Thus, we aim to consider a fully self-consistent picture assuming that any accretion disc that was present before TDE had insignificant mass and so could be neglected.

In the analytic treatment given below, we assume that the disc mid-plane is everywhere close to the black hole equatorial plane, while the plane in which the unperturbed stream moves coincides with the orbital plane of the disrupted star and is inclined at an angle β_* with respect to the black hole's equatorial plane. We introduce a Cartesian coordinate system (XYZ) with origin at the black hole location. The (XY) plane coincides with the equatorial plane of the black hole. The angle between the X-axis and the line of intersection of the plane containing the stream with the equatorial plane of the black hole is γ_*.

In the same way, we define the inclination of the disc mid-plane at radius R to be $\beta(t, R)$ and the angle between the line of intersection of this plane and the (XY) plane and the X-axis to be $\gamma(t, R)$. In the analysis presented below, it is very convenient to work with the complex variables $\mathcal{W}(t, R) = \beta(t, R)e^{{\rm i}\gamma(t,R)}$ and $\mathcal{W}_* = \beta_* e^{{\rm i}\gamma_*}$. Hereafter, we use calligraphic letters for complex quantities. The angles β and γ are associated with a tilt of the local disc angular momentum vector such that the angle between this vector and the Z-axis is β and the angle between its projection on the (X, Y) plane and the X-axis is $\pi/2 - \gamma$. This tilt produces a displacement of a disc fluid element in the Z direction which in the case of small β, which will be considered below, is equal to $\beta(Y - {\rm i}X)\exp(-{\rm i}\gamma)$.

When the disc is flat, the angles β and γ are obviously constant. It is one of the purposes of this paper to find the conditions under which these angles have a significant dependence on radius and time due to the influence of stream on the disc.

An important aspect of the problem on hand is that physical processes arising from three distinctive phenomena interact with each other. These are associated with the stellar orbit and the stream of gas, the dynamics of the accretions disc and relativistic effects determined by the gravitational field of the black hole, respectively. Accordingly, we define important quantities characterizing these three types of processes and introduce characteristic temporal and spatial scales for them in turn. A list of the main parameters and symbols used in this paper is given in Table 1.

2.1 Characteristic spatial and temporal scales and basic quantities associated with the stellar orbit and gas stream

We now specify spatial and temporal scales associated with the stellar orbit and the gas stream. For unit of distance, we use either the periastron distance $R_{\rm p}$ of the initial stellar orbit or the distance of the location where the stream impacts the disc from the black hole, $R_{\rm S}$. In general, we have $R_{\rm S} > R_{\rm p}$. When the disc is sufficiently inclined with respect to the plane of the stellar orbit as can arise for a black hole that rotates sufficiently rapidly, we typically have $R_{\rm S} \sim R_{\rm p}$. These distances are expressed as multiples of the tidal radius, $R_{\rm T}$, with the multiplication factors being $1/B_{\rm p}$ and $1/B_{\rm S}$, respectively. The quantities $B_{\rm p}$ and $B_{\rm S}$ are described as penetration factors.[5] The tidal radius is given by

$$R_{\rm T} = (M/m)^{1/3}\, R_* = 7 \times 10^{12} M_6^{1/3}\,{\rm cm} = 46 M_6^{-2/3} R_{\rm g}, \quad (1)$$

where M and m are the masses of black hole and star, respectively, R_* is the stellar radius, $M_6 = M/10^6\,{\rm M}_\odot$, and we define the gravitational radius as $R_{\rm g} = GM/c^2$, where c and G are the speed of light and the gravitational constant. In what follows below, we shall assume that m and R_* have solar values. We then have $R_{\rm p} = R_{\rm T}/B_{\rm p}$ and $R_{\rm S} = R_{\rm T}/B_{\rm S}$.

There are several important temporal scales associated with the orbit and the stream. First, there are the inverse Keplerian angular frequencies at the stream impact position and at periastron. The former is given by

$$t_{\rm S} \equiv \Omega_{\rm S}^{-1} = \frac{R_{\rm S}^{3/2}}{\sqrt{GM}} = \frac{R_*^{3/2}}{\sqrt{Gm}} B_{\rm S}^{-3/2} \equiv B_{\rm S}^{-3/2} t_* = 1.6 \times 10^3 B_{\rm S}^{-3/2}\,{\rm s}, \quad (2)$$

and the latter by

$$t_{\rm p} \equiv \Omega_{\rm p}^{-1} = \frac{R_{\rm p}^{3/2}}{\sqrt{GM}} = \frac{R_*^{3/2}}{\sqrt{Gm}} B_{\rm p}^{-3/2} \equiv B_{\rm p}^{-3/2} t_* = 1.6 \times 10^3 B_{\rm p}^{-3/2}\,{\rm s}. \quad (3)$$

Secondly, there is the minimal return time of the stellar material in the stream to periastron after the disruption of the star. This is estimated as

$$P_{\rm min} = \frac{\pi}{\sqrt{2}} (R_{\rm p}/R_*)^3\, (m/M)^{1/2}\, t_* = 3.5 \times 10^6 M_6^{1/2} B_{\rm p}^{-3}\,{\rm s}. \quad (4)$$

This is simply the period of an orbit with semi-major axis equal to $R_{\rm p}^2/(2R_*)$. This orbit has a binding energy per unit mass equal to the change in potential energy per unit mass experienced when moving a distance R_* towards the black hole from pericentre. This gives the greatest specific binding energy that material originating from the disrupted star is expected to have. After the minimal return time, the disc accretes matter from the stream at a rate that can be estimated as

$$\dot{M}_{\rm S} = \frac{0.5m}{P_{\rm min}} \left(\frac{t}{P_{\rm min}}\right)^{-5/3} = 2.8 \times 10^{26} B_{\rm p}^3 \left(\frac{t}{P_{\rm min}}\right)^{-5/3}\,{\rm g\,s^{-1}}. \quad (5)$$

We remark that this follows under the assumption that the mass that has been accreted at any stage is all that was more strongly bound than the material currently returning to periastron together with the additional assumption that there is a linear relation between the specific binding energy of returning material and the total mass of material that was more strongly bound and has returned previously (see e.g. Rees 1988).

[5] In the literature, $B_{\rm p}$ is often denoted by β, see e.g. Carter & Luminet (1983, 1985). We use the symbol B to distinguish these quantities from the inclination angles.

2.2 Torques acting between stream and disc

The unit vector in the direction of the angular momentum at a point in the disc expressed in the (XYZ) coordinate system is given by

$$\hat{\boldsymbol{l}} = (\sin(\beta(t,R))\sin(\gamma(t,R)), -\sin(\beta(t,R))\cos(\gamma(t,R)), \cos(\beta(t,R))). \quad (6)$$

The corresponding unit vector for the stream is

$$\hat{\boldsymbol{l}}_* = (\sin(\beta_*)\sin(\gamma_*), -\sin(\beta_*)\cos(\gamma_*), \cos(\beta_*)). \quad (7)$$

The rate of change of the component of the disc angular momentum in the (X, Y) plane as a result of interaction with the stream is

$$\dot{\boldsymbol{L}} = \dot{M}_{\rm S} J_{\rm S} (\hat{\boldsymbol{l}}_* - \hat{\boldsymbol{k}}(\hat{\boldsymbol{l}}_* \cdot \hat{\boldsymbol{k}})), \quad (8)$$

where $J_{\rm S} = \sqrt{2GMR_{\rm p}}$ is the specific angular momentum of the stream material which corresponds to that associated with a parabolic orbit with pericentre distance $R_{\rm p}$ and $\hat{\boldsymbol{k}}$ is the unit vector in the Z direction. We now assume that the inclinations β and β_* are of small magnitude. Then with the help of equation (8), to first order in β_* we may write

$$\dot{\mathcal{L}} = \sqrt{GMR_{\rm S}}\,\dot{M}_{\rm S} \lambda \mathcal{W}_*, \quad (9)$$

where $\dot{\mathcal{L}} = {\rm i}\dot{L}_X - \dot{L}_Y$. Here we have written $\boldsymbol{L} = (L_X, L_Y, L_Z)$ and $\lambda = \sqrt{2R_{\rm p}/R_{\rm S}} = \sqrt{2B_{\rm S}/B_{\rm p}}$. To find the torque acting so as to change the specific angular momentum of the disc material, we must subtract a contribution corresponding to inserting the stream material with the same specific angular momentum as the local disc. Thus, with the help of equation (7) we obtain that correct to first order in small quantities this torque is given by

$$\mathcal{T} = \sqrt{GMR_{\rm S}}\,\dot{M}_{\rm S}(\lambda \mathcal{W}_* - \mathcal{W}). \quad (10)$$

To consider further the influence on the disc, we need to specify how the influence of the stream is distributed. Hereafter, we assume that it is concentrated in a narrow region around $R_{\rm S}$ of size $\Delta R_{\rm S} \ll R_{\rm S}$, and, accordingly, that consequent torques can be approximated as being proportional to $\delta_\Delta\,(1 - R/R_{\rm S})/R_{\rm S}$, where $\Delta = (\Delta R_{\rm S})/R_{\rm S}$. Here $\delta_\Delta(x)$ is the so-called 'nascent' delta function. This is an even function of x such that $\int_{-\infty}^{+\infty} {\rm d}x \delta_\Delta(x) = 1$, and it converges to the Dirac delta function in the limit $\Delta \to 0$.

Adopting the above assumptions and definitions, it is easy to see that we may write

$$\mathcal{T} = \int 2\pi \Sigma R \sqrt{GMR}\,\dot{\mathcal{W}}_*\,{\rm d}R, \quad (11)$$

where the disc surface density is Σ, the integral is taken over the disc and $\dot{\mathcal{W}}_*$ has the form

$$\dot{\mathcal{W}}_* = \frac{\dot{M}_{\rm S}}{2\pi\Sigma R^2} (\lambda \mathcal{W}_* - \mathcal{W}) \delta_\Delta (1 - R/R_{\rm S}). \quad (12)$$

Note that the parameter λ is expected to be unity when the specific angular momentum at the circularization radius is the same as that of the stream material. Then we see from equation (12) that $\dot{\mathcal{W}}_* = 0$ when the orbital planes of the stream and disc are aligned as expected. We assume, for simplicity, that this condition is valid, and therefore set $\lambda = 1$ in the remainder of the paper.

2.3 Basic quantities associated with the dynamics of the accretion disc

For our purposes, we need to know the evolution of disc aspect ratio, $\delta = H/R$, with H being the local semi-thickness. In general, δ and Σ are both functions of time and radial distance. Immediately after the disc has been formed, it is expected that it will evolve in the advection-dominated slim disc regime and $\delta \sim 1$. At later stages of evolution, when the accretion rate gets smaller than the Eddington limit, the disc becomes radiative and δ is expected to be quite small, $\delta \sim 10^{-3}$.

We adopt the usual assumption that the evolution of the disc's basic quantities is governed by a turbulent viscosity modelled through the α prescription, where kinematic viscosity ν takes the form

$$\nu = \alpha\delta^2\sqrt{GMR}, \tag{13}$$

where the viscosity parameter $\alpha < 1$ is a constant. In general, we solve equations determining $\Sigma(t, R)$ and $\delta(t, R)$ numerically, see Section 5 below for a description of our method, and use the obtained values as inputs for our analytic model for the evolution of the disc tilt and twist. We choose the unit of surface density, Σ_0, to be determined by the stellar mass and the stream impact distance according to $\Sigma_0 = m/(2\pi R_{\rm S}^2)$. We then use the dimensionless surface density $\tilde{\Sigma} = \Sigma/\Sigma_0$ below.

2.4 Basic quantities determined by relativistic effects

Since the spatial scales we consider are assumed to be significantly larger than the gravitational radius, we treat the influence of relativistic effects through additional effective forces acting in the classical Newtonian description. Accordingly, our SPH simulations are performed using the expression for the gravitational acceleration due to the black hole, $\boldsymbol{a}$, given by

$$\boldsymbol{a} = -\nabla\Phi + \boldsymbol{F}_{\rm GM}. \tag{14}$$

The potential Φ is determined by the Newtonian potential with the addition of a correction which leads to the apsidal precession of close free particle orbits. Thus

$$\Phi = -\frac{GM}{R} - 3\frac{G^2M^2}{c^2R^2}. \tag{15}$$

The form of this correction is chosen so as to provide the same rate of apsidal precession as the expected relativistic Einstein precession (Garavaglia 1987). Note that our hydrodynamical simulations employ another form of potential proposed by Paczyński & Wiita (1980). Although the Paczyński–Wiita potential gives the wrong rate of apsidal precession, it gives the correct radius for the last stable orbit in the case of a Schwarzschild black hole. The reason for these choices was that apsidal precession is potentially significant for a tilted twisted disc at large distances but less so for an accreting aligned disc for which the location of the last stable orbit may play a more important role.

The gravitomagnetic force per unit mass $\boldsymbol{F}_{\rm GM}$ represents the effect of frame dragging (see e.g. Thorne, Price & Macdonald 1986). It takes the form

$$\boldsymbol{F}_{\rm GM} = \boldsymbol{v}\times\boldsymbol{B}, \quad \boldsymbol{B} = \Omega_{\rm LT}(R)\left(\hat{\boldsymbol{k}} - 3\frac{(\hat{\boldsymbol{k}}\cdot\boldsymbol{R})\boldsymbol{R}}{R^2}\right), \tag{16}$$

where $\cdot$ represents the scalar product, the unit vector $\hat{\boldsymbol{k}}$ is along the Z-axis of the (XYZ) coordinate system and $\boldsymbol{R}$ is the position vector such that $R = |\boldsymbol{R}|$. The Lense–Thirring frequency given by

$$\Omega_{\rm LT} = 2a\frac{G^2M^2}{c^3R^3} \tag{17}$$

determines the precession rate of circular orbits of radius $R \gg R_{\rm g}$ that is slightly inclined to the equatorial plane. It is proportional to black hole rotation parameter a. This parameter a lies in the range $-1 \geq a \geq 1$, with negative values corresponding to the situation when black hole rotates in the direction opposite to that of orbital motion. When the black hole is non-rotating, $a = 0$.

3 THE GOVERNING EQUATION FOR A TWISTED TILTED DISC

In what follows, we assume that the disc aspect ratio δ and surface density Σ change on a time-scale that is much longer than the time-scale associated with evolution of the disc inclination and orientation angles β and γ. Under this assumption, we can solve an equation for the quantity $\mathcal{W} = \beta e^{{\rm i}\gamma}$, assuming that a steady state has been set up, in order to find twisted tilted disturbances of the disc induced by the stream for which there is no explicit dependence on time.

Such a governing equation has been derived by several authors under various simplifying assumptions (see e.g. Papaloizou & Pringle 1983; Papaloizou & Lin 1995; Demianski & Ivanov 1997; Ivanov & Illarionov 1997). In this paper, we adopt the form obtained by Ivanov & Illarionov (1997, hereafter II), who assumed that β, α, δ and the ratio of gravitational radius to a radius of interest are all small. This takes the form

$$\frac{\delta^2\sqrt{GM}}{4\alpha\xi R}\frac{\mathrm{d}}{\mathrm{d}R}\left(\xi R^{3/2}\frac{(1+{\rm i}k)}{(1+k^2)}\frac{\mathrm{d}\mathcal{W}}{\mathrm{d}R}\right) + {\rm i}\Omega_{\rm LT}\mathcal{W} + \dot{\mathcal{W}}_* = 0, \tag{18}$$

where

$$k = \frac{3GM}{c^2\alpha R} \tag{19}$$

determines the contribution of post-Newtonian corrections to the equation of motion. The last term in equation (18) describes the influence of the stream on the disc. It is given by equation (12) and is absent in II. The factor $\xi = \Sigma\delta^2R^{1/2}$ is approximately constant for a 'standard' thin accretion discs sufficiently far from the last stable orbit. For such a disc, the inward advective flow of angular momentum is approximately balanced by outward angular momentum flow transferred by viscous forces, and, in this case ξ is proportional to the flux of mass in the disc. In our case, there is a mass inflow in the disc due to the presence of the stream, and the disc is, in general, time dependent and may be moderately thick. Thus, ξ is retained in our numerical solutions of equation (19), where both δ and ξ are taken from a background numerical model, see below. However, we set $\xi = {\rm const}$ in our analytic estimates for simplicity.

Note that equation (18) implies time dependence only implicitly, through the factors δ, ξ and $\dot{\mathcal{W}}_*$, which are, in general, functions of time. This is approximately valid when characteristic time-scales associated with the evolution of disc's tilt and twist are much smaller than the ones corresponding to the background quantities and $\dot{\mathcal{W}}_*$. This condition may be broken in course of evolution of our system, especially during the transition of disc from 'high' state with a large $\delta \sim 1$ to a low state with $\delta \ll 1$, when the thermal instability may operate on a relatively short time-scale $t_{\rm TH} \sim \alpha^{-1}t_{\rm S}$ and sharp features in distribution of ξ and δ may propagate over the disc on the sound crossing time-scale $t_{\rm sound} \sim \delta^{-1}t_{\rm S}$. When $\alpha > \delta$, both $t_{\rm TH}$ and $t_{\rm sound}$ are smaller than a characteristic time-scale of tilt and

twist diffusion $t_{\rm TW} \sim (\alpha/\delta)t_{\rm S}$. In the opposite limit, tilt and twist have a typical propagation time of the order of $t_{\rm sound}$ and dissipation time-scale of the order of $t_{\rm TH}$. Clearly, the assumption of a stationary twisted disc may not be valid when it is undergoing rapid transitions in either case. However, the stationary states represent the target states that the disc evolves towards at any time and so we shall make the assumption in this paper in order to obtain an estimate of typical possible disc inclinations and their dependence on the parameters of the problem as a first step towards constructing more realistic time-dependent models of a twisted disc under the influence of a gas stream.

All the terms in equation (18) correspond to projections of torques induced in the disc on to the equatorial plane, divided by the value of Keplerian angular momentum stored in the disc per unit radius which is given by $\mathrm{d}L/\mathrm{d}R = 2\pi\Sigma R\sqrt{GMR}$. These projections enter equation (18) in combinations $\mathcal{T} = \mathrm{i}T_X - T_Y$, where $T_{X,\,Y}$ are X and Y components of the torques (see for example Section 2.2).

It is convenient to introduce dimensionless radial distance $r = R/R_{\rm S}$ and rewrite equation (18) in the form

$$\frac{1}{r\xi}\frac{\mathrm{d}}{\mathrm{d}r}\left(r^{3/2}\xi\frac{(1+\mathrm{i}k)}{(1+k^2)}\frac{\mathrm{d}\mathcal{W}}{\mathrm{d}r}\right) \pm \mathrm{i}\frac{\eta^{3/2}}{r^3}\mathcal{W} + \sigma(\mathcal{W}_* - \mathcal{W})\delta_\Delta(r-1) = 0, \tag{20}$$

where the positive (negative) sign corresponds to prograde (retrograde) rotation of the black hole with respect to the disc gas; we have used equation (12) and $\mathcal{W}_* = \lambda\mathcal{W}_*$.

In addition $\eta = R_{\rm BP}/R_{\rm S} = \frac{2}{23}B_{\rm S}(\alpha|a|M_6\delta^{-2})^{2/3}$

with $R_{\rm BP} = 4(\alpha|a|)^{2/3}\delta^{-4/3}\frac{GM}{c^2}$, (21)

and

$$\sigma = \frac{4\alpha}{\delta^2}\frac{\dot{M}_{\rm S}}{2\pi\Sigma R_{\rm S}^2}\sqrt{\frac{R_{\rm S}^3}{GM}}. \tag{22}$$

3.1 Important parameters determining the response of the disc to the incoming stream

The quantity σ can be simply interpreted as the ratio of the time-scale for warp diffusion over the length-scale $R_{\rm S}$ to the local mass accretion time-scale. Its value is accordingly expected to be important for determining the expected disc misalignment produced by a misaligned stream. A large value implies that warp propagation should be ineffective at dispersing accreting misaligned angular momentum and thus favour a misaligned disc. Note in addition that $R_{\rm BP}$ characterizes the scale of disc alignment with the equatorial plane of the black hole at small radii in the absence of the stream. This always occurs when the relativistic correction parameter k may be neglected. The parameter $\eta = R_{\rm BP}/R_{\rm S}$ measures the importance of the tendency towards alignment at the stream impact radius and therefore its value is important for determining the disc response, a large value favouring alignment. The tendency towards alignment with the black hole equatorial plane is known as the Bardeen–Petterson effect (Bardeen & Petterson 1975).

However, this does not operate in the disc when $\alpha < \alpha_{\rm crit} = |a|^{-2/5}\delta^{4/5}$ and the black hole rotation is prograde, $a > 0$, see II. In that case, the relativistic correction parameter, k, is important and there are oscillations of the inclination angle at small radii instead of alignment (see also Demianski & Ivanov 1997; Lubow, Ogilvie & Pringle 2002; Zhuravlev & Ivanov 2011, hereafter ZI; Morales Teixeira et al. 2014; Zhuravlev et al. 2014). In the case of retrograde rotation, alignment can take place at all reasonable values of α. When $\alpha < \alpha_{\rm crit}$, the alignment scale differs from $R_{\rm BP}$, and it does not depend on α (see II). This typical radial scale, $R_{\rm rel}$, together with the ratio $\eta_{\rm rel} = R_{\rm rel}/R_{\rm S}$, which plays the role of η in this case, can be defined as

$$R_{\rm rel} = 4|a|^{2/5}\delta^{-4/5}\frac{GM}{c^2}, \quad \text{with}$$

$$\eta_{\rm rel} = R_{\rm rel}/R_{\rm S} = \frac{2}{23}B_{\rm S}|a|^{2/5}M_6^{2/3}\delta^{-4/5}. \tag{23}$$

3.2 Numerical solutions of the governing equation

3.2.1 *Boundary conditions and solution method*

In general, equation (20) should be solved numerically. In order to do that, we need to specify the inner and outer boundary conditions. As the outer boundary condition at some outer radius of the computation domain $r_{\rm out}$, we adopt $\mathrm{d}\mathcal{W}/\mathrm{d}r = 0$ to mimic a regularity condition at the disc outer edge. In general, the inner boundary condition set at an inner radius of the computation domain, $r_{\rm in}$, should be different according to whether solutions of the homogeneous form of equation (20) (for which $\mathcal{W}_* = 0$) possess growing and decaying modes (i.e. when either $a > 0$ and $\alpha > \alpha_{\rm crit}$ or $a < 0$) or when the solutions are oscillatory ($a > 0$ and $\alpha < \alpha_{\rm crit}$).

However, in the former case, a precise form of the inner condition is actually not important. Indeed, when the equation is numerically integrated from $r_{\rm in}$ towards larger radii, its solution rapidly converges to the growing mode regardless of the form of the inner boundary condition. In the latter case, setting a different boundary condition would only lead to a different phase of the oscillations, which should not influence our qualitative results. Therefore, in this paper, for simplicity, we adopt $\mathrm{d}\mathcal{W}/\mathrm{d}r = 0$ at the inner radius of computational domain as well. Note that such inner and outer boundary conditions ensure that disc's inclination vanishes when the forcing term due to the stream disappears.

In order to obtain a solution with the specified inner and outer boundary conditions, we employ a fitting point procedure. To do this, we solve both the homogeneous and inhomogeneous forms of equation (20) starting from $r_{\rm in} \ll 1$ and ending at $r = 1$, and also starting from $r_{\rm out} \gg 1$ and ending again at $r = 1$. We then choose multiplication coefficients for the homogeneous solutions which are such as when these are added in, the requirement of continuity of the solution and its radial derivative at $r = 1$ is satisfied. When such procedure is used, it is evident that a precise form of inner and outer boundary conditions does not play a significant role in all cases for which growing and decaying modes exist, since they are singled out by the numerical procedure.

3.2.2 *Numerical results for constant δ*

Solutions of equation (20) using time-dependent background numerical models based on either SPH or finite difference scheme are discussed in the subsequent sections. Here we consider models with constant δ and ξ as they provide qualitative information on the possible behaviour of more complicated cases.

Solutions of equation (20) obtained under the assumptions stated above are shown in Figs 1 and 2 for the case with $\alpha > \alpha_{\rm crit}$ and in Fig. 3 for the case with $\alpha < \alpha_{\rm crit}$. In the former case, we present solutions representing each of the four regimes which correspond

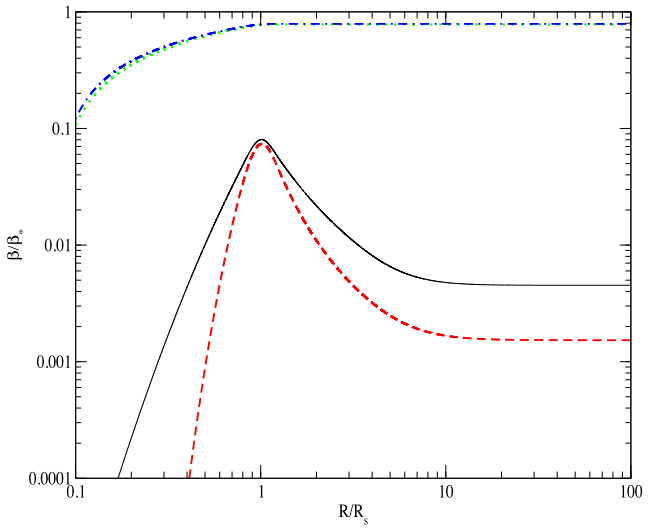

Figure 1. The dependence of inclination angle β in units of its maximal β_* on radius is shown. Cases with $\alpha > \alpha_{\rm crit}$ and $\sigma = 1$ are illustrated. The parameters corresponding to the different curves are given in the text.

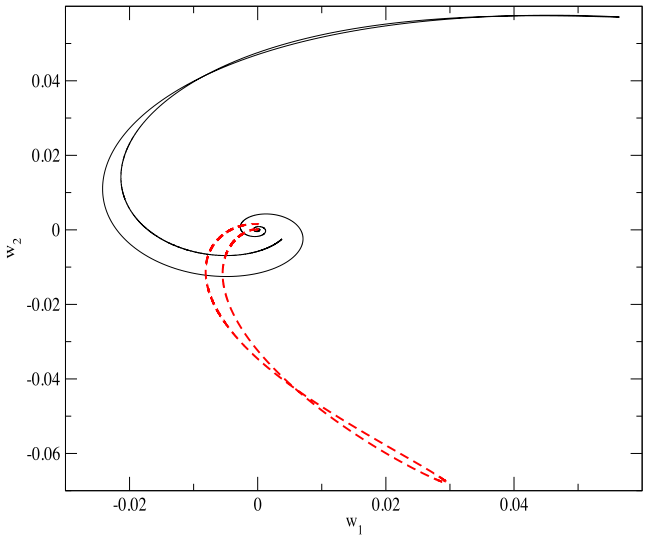

Figure 2. A parametric representation of the solutions corresponding to $\eta = 8.7$ shown as curves on the plane $[w_1 = {\rm Re}(\mathcal{W}), w_2 = {\rm Im}(\mathcal{W})]$. Solid and dashed curves show the cases with $a > 0$ and $a < 0$, respectively. For more details, see the text.

to positive and negative values of a together with values of η greater and less than unity. In the latter case, an analogous set of four cases, defined as in the former case, are considered, the only difference being that η is replaced by $\eta_{\rm rel}$. In all of these cases, we set $\sigma = 1$. We go on to discuss the dependence of a typical inclination angle on values of σ below.

In Fig. 1, the inclination angle β is shown in units of its maximal theoretically expected value $\beta_* = |\mathcal{W}_*|$ as a function of r, for the cases when $\alpha > \alpha_{\rm crit}$. As $\lambda = 1$, $\beta_* = |\mathcal{W}_*|$ corresponds to the case where the disc and stream orbital planes are aligned. In the absence of warp or twist propagation, the stream is not expected to misalign the disc with respect to the equatorial plane of the black hole to a greater extent.

Solid and dashed lines respectively correspond to prograde and retrograde black hole rotation. For these cases, $\alpha = 0.1$, $\delta = 0.01$,

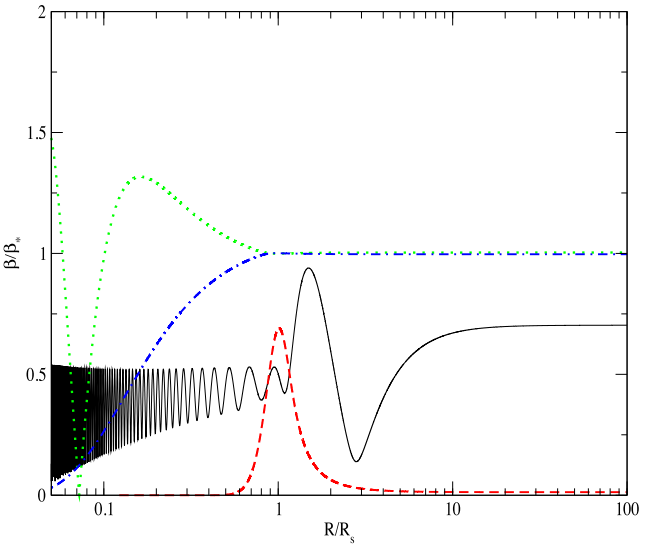

Figure 3. As in Fig. 1 but for the cases with $\alpha < \alpha_{\rm crit}$. The parameters corresponding to the different curves are given in the text.

$|a| = 1$, $M_6 = 1$, accordingly, $\eta = 8.7 > 1$ and $\eta_{\rm rel} = 3.5$. Dotted and dot–dashed lines show solutions for prograde and retrograde rotation for the case of small $\eta = 0.2$. The other parameters for these are $\alpha = 0.5$, $\delta = 0.056$, $|a| = 1$, $M_6 = 0.02$ and $\eta_{\rm rel} = 6.4 \times 10^{-2}$. One can see that when η is fixed the curves corresponding to $a > 0$ and $a < 0$ are almost indistinguishable. For both large and small η, the disc aligns with the equatorial plane at small r. However, when $r > 1$, these cases behave differently. When η is large, the inclination angle drops to values much smaller than the maximal value at $r = 1$ at larger radii. On the other hand, for small η, the inclination angle is approximately constant at $r > 1$. These results simply represent the effect of the alignment radius moving outwards as η is increased and so causing the disc to align at larger radii.

Fig. 2 shows the trajectory of the prograde and retrograde solutions having $\eta = 8.7$ on the plane $[w_1 = {\rm Re}(\mathcal{W}), w_2 = {\rm Im}(\mathcal{W})]$ with r as parameter. Note that for small inclinations the radial and angular polar coordinates corresponding to $w_1(r)$ and $w_2(r)$ are $|\beta|$ and γ, respectively. Both curves have their origin at $r = r_{\rm min}$. When r grows, but is less than unity, the curve corresponding to $a > 0$ ($a < 0$) spirals clockwise (anticlockwise), but the direction of evolution changes when r becomes greater than unity. That means that when $r < 1$ the rotation of the polar angle γ is always directed in the sense of the black hole rotation, see also II and ZI.

Fig. 3 shows the evolution of the inclination angle when $\alpha < \alpha_{\rm crit}$ and the relativistic correction k determines the shape of the disc. Solid and dashed curves represent the case of large $\eta_{\rm rel} = 5 > \eta = 1.72$ for prograde and retrograde rotation of the black hole, respectively. Other parameters corresponding for these cases are $\alpha = 3.5 \times 10^{-3}$, $\delta = 6.3 \times 10^{-3}$, $|a| = 1$ and $M_6 = 1$. Dotted and dot–dashed curves illustrate the cases with relatively small $\eta_{\rm rel} = 0.2 > \eta = 3 \times 10^{-3}$ for prograde and retrograde black hole rotation, respectively. Other parameters were $\alpha = 3.5 \times 10^{-3}$, $\delta = 6.3 \times 10^{-3}$, $|a| = 1$ and $M_6 = 1$. The most important difference between these cases and those with $\alpha > \alpha_{\rm crit}$ is that the disc does not align at small radii when the black hole rotation is prograde. Instead, there are radial oscillations of the inclination angle with wavenumber and amplitude increasing towards black hole, see II. This effect is much more prominent in the cases with large $\eta_{\rm rel}$. Note, however,

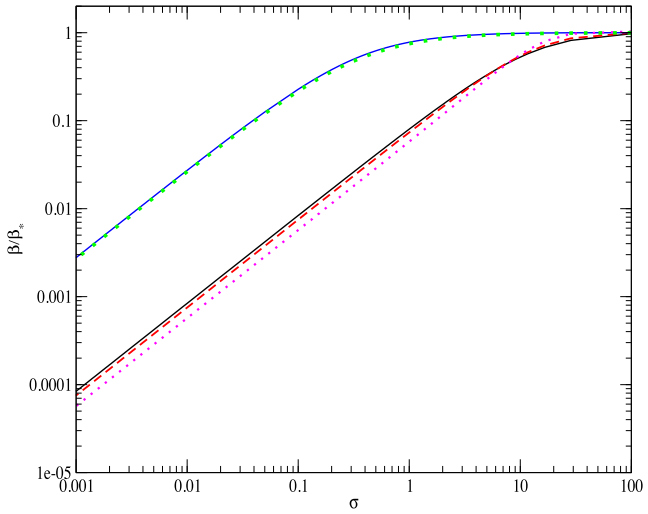

Figure 4. The dependence of the disc inclination at the stream impact position, β_S, is shown as a function of the parameter σ for two disc's models specified in the text as cases 1 and 2, where $\alpha > \alpha_{crit}$. The solid line with a smaller value of β_S at a given r and the dashed line represent numerical solutions of equation (20) corresponding to case 1 with $a = 1$ and -1, respectively. The dotted curve with a smaller value of its argument is for the same case, but calculated with the help of equation (A9). Solid and dotted lines with larger values of their arguments are for case 2. The solid line is calculated numerically, while the dotted one is given by equation (A11). Both lines correspond to $a > 0$.

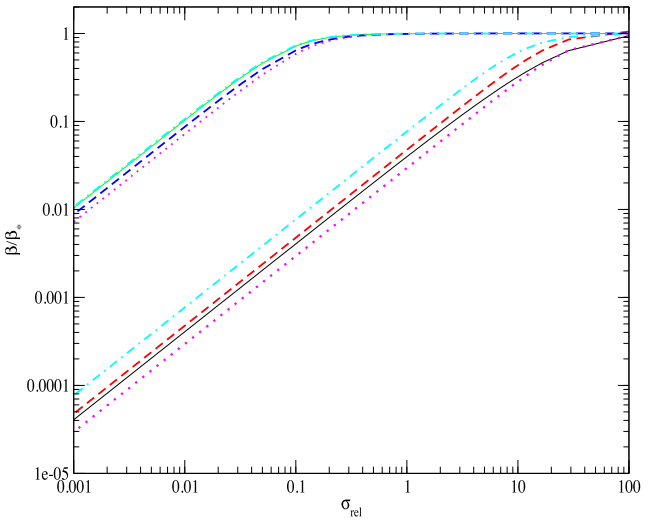

Figure 5. Same as Fig. 4, but for the cases 2 and 3 having $\alpha < \alpha_{crit}$ and β_S is shown as a function of $\sigma_{rel} = k\sigma$, see the text for a description of particular curves.

that in this case the approximations leading to equation (20) fail to be valid at radii $r \ll \eta_{rel}$ and, therefore, oscillations in the disc inclination with radial wavenumber $\gg 1/R_{rel}$ are likely to be absent. We remark that values of β at $r = 1$ are approximately the same for curves corresponding to the same η_{rel}.

We now go on to make a comparison of numerical solutions to equation (20) with those obtained using a simple analytic approach developed in Appendix A. The cases having $\eta = 8.7$, 0.2 and $\eta_{rel} = 5$, 0.2 will be hereafter referred to as cases 1–4, respectively. The appropriate values of α, δ and M_6 are specified above.

In Fig. 4, we show a comparison of our analytic approach with numerical solutions of equation (20) having $\alpha > \alpha_{crit}$. We plot the dependence of the disc inclination at the stream impact position, β_S, in units of β_* as a function of the parameter σ. For the case with $\eta = 8.7 > 1$ (case 1), we show two numerical curves corresponding to prograde and retrograde black hole rotations. A typical deviation of these curves from the result following from equation (A9) is about 30 per cent. For the case with small $\eta = 0.2 < 1$ (case 2), curves corresponding to prograde and retrograde rotations practically coincide; therefore, only the one with $a > 0$ is shown. The analytic result following from equation (A11) is also very close to the numerical curves. We remark that β_S becomes significant for large σ. As σ is a measure of the warp diffusion time to the accretion time, this is as expected.

In Fig. 5, we show results of a corresponding comparison between numerical results for the cases 3 and 4 with $\alpha < \alpha_{crit}$ and those obtained from our analytic expression (A6). Here we plot the dependence of the disc inclination at the stream impact position, β_S, as a function of the parameter $\sigma_{rel} = k\sigma$.

The uppermost curves of a given type correspond to case 3 for which $\eta_{rel} = 5$ is relatively large, while lowermost curves of a given type correspond to case 4 for which $\eta_{rel} = 0.2$ is small. Solid and dashed lines respectively show numerical results for prograde and retrograde rotation, while dotted and dot–dashed lines are obtained analytically for $a = 1$ and -1. One can see that the disagreement between numerical and analytic results in this case is now of the order of 30–40 per cent. This means that the simplified analytic solutions are accurate enough for our purposes.

Note that so far we have considered only solutions corresponding to the case of constant δ. In our numerically obtained models of background quantities, two qualitatively different dependences of δ on r arise during a period of transition from a 'high' to 'low' state. Since this transition initially occurs at larger radii, there are configurations with δ being order of unity at radii smaller than some 'transition' radius $r_{tr} > 1$, and $\delta \sim 10^{-3}$ for $r > r_{tr}$. When the transition happens at radii of $r \sim 1$, there appear distributions of δ in the low state $\delta \sim 10^{-3}$ at radii both smaller and larger than 1, while at $r \sim 1$, δ can be significantly larger than its typical 'low' value due to heating of the disc gas through the input of kinetic energy carried by the stream. Such configurations have an intermittent nature through the development of thermal instability, provided that radiation pressure dominates over the disc gas pressure and the α prescription for viscosity is assumed to be valid. In principle, they can also be treated by a technique similar to that used in Appendix A for the case of constant δ. However, here, for simplicity, we do not consider these more complicated cases leaving them for a future work.

4 SPH SIMULATIONS OF DISCS SUPPLIED BY A STREAM RESULTING FROM TIDAL DISRUPTION

We have performed SPH simulations of the evolution of a disc which is impacted by a gaseous stream resulting from tidal disruption of a star. We use a modified version of the publicly available code GADGET-2 (Springel 2005). This is a hybrid *N*-body/SPH code capable of modelling both fluid and distinct massive bodies that interact with it.

In our case, we incorporate a rotating black hole of fixed mass *M*. Relativistic effects are incorporated by adding effective forces acting within a classical Newtonian description (see Section 2.4). We adopt spherical polar coordinates (R, θ, ϕ) with origin at the

location of the black hole. The associated Cartesian coordinates (X', Y', Z') are chosen such that the (X', Y') plane coincides with initial orbital plane of the tidally disrupted star. In addition, the location of the Y'-axis is chosen such that the angular momentum vector of the black hole is given by $\boldsymbol{J} = (0, J\sin(i), J\cos(i))$, where $J = aGM^2/c$, with a being the black hole rotation parameter and i is the inclination of this vector to the Z'-axis. We recall that $\boldsymbol{J}$ defines the direction of the Z-axis for the coordinate system with (X, Y) plane coinciding with the equatorial plane of the black hole that we adopted in Section 2. In this section, for convenience we shall choose the X-axis to coincide with the X'-axis which corresponds to γ_* defined in Section 2 taken to be zero. For our simulations, we take the penetration factor $B_\mathrm{p} = 5/3$, $i = \pi/4$ and $M = 10^6\,\mathrm{M}_\odot$.

The dimensionless time unit for these calculations was taken to be the inverse periastron frequency Ω_p^{-1} and in this section the dimensionless unit of length is taken to be the periastron distance R_p; thus, R expressed in dimensionless units is $r_\mathrm{p} = R/R_\mathrm{p}$.

The gaseous disc and the stream are represented by SPH particles. The total unsoftened gravitational potential Φ at a position $\boldsymbol{R}$ is given by equation (15) and the gravitomagnetic force per unit mass by equation (16). An important issue for N-body/SPH simulations is the choice of the gravitational softening lengths. The only gravitational softening that is included in our simulation applies to the gravitational interaction between the SPH particles and the black hole. For the practical computation of the gravitational interaction between the black hole and the gas particles, the potential and gravitomagnetic force were softened following the method of Springel (2005). This was implemented with fixed softening length $\varepsilon = 0.05$ in dimensionless units. Shocks were handled following the procedure of Springel (2005). In particular, the parameter α that scales the magnitude of the applied viscous force that is defined in equation (14) of Springel (2005, but which is not used in that context elsewhere in this paper) was chosen to be 0.5. Furthermore, the black hole was assumed to accrete gas particles that approach it to within 0.1 dimensionless units. Thus, such particles were removed from the simulation. In addition, the gravitational effect of the disc on the black hole is neglected.

4.1 Initial conditions

4.1.1 Disc setup

The disc setup is such that the angular momentum vector for all particles was in the same direction enabling a mid-plane for the disc to be defined. This mid-plane is set up such that the disc's total angular momentum vector is parallel to the magnetic spin vector of the black hole. The particle distribution was chosen to model a disc with surface density profile given by

$$\Sigma = \Sigma_1 R^{-1/2}. \tag{24}$$

Here Σ_1 is a constant. The disc mass is then given by

$$M_\mathrm{D} = 2\pi \int_{R_\mathrm{in}}^{R_\mathrm{out}} \Sigma(r') r' \mathrm{d}r' = \frac{4}{3}\pi\Sigma_1 R_\mathrm{out}^{3/2}, \tag{25}$$

where R_in and R_out are the inner and outer disc boundary radii. When these and the disc mass are specified, equation (25) is used to determine Σ_1. For the simulations presented here, we adopted $M_\mathrm{D} = 0.2m$, $R_\mathrm{in} = 0.5$ and $R_\mathrm{out} = 1$ with the last two being given in dimensionless units. As self-gravity is expected to play a minor role, it is neglected in the simulations. The disc was evolved for several hundred time units in order to attain a relaxed quasi-steady distribution before being allowed to interact with a mass stream.

4.1.2 Setting up the star at pericentre and generation of the mass stream

We adopt a simple procedure for generating a stream generated that might be expected to arise from a tidally disrupted star that subsequently provides a mass source for a disc that is formed partly from pre-existing material as well as that from the stream. The particles comprising a 'star' are initially set up so as to form a homogeneous sphere of radius $\mathrm{R}_\odot$ with its centre of gravity at the pericentre location given in Cartesian coordinates by $\boldsymbol{R}_0 = (R_\mathrm{p}, 0, 0)$. Particles with $|\boldsymbol{R}| > R_\mathrm{p}$ are reflected according to

$$\boldsymbol{R} = \left(X', Y', Z'\right) \rightarrow \left(2R_\mathrm{p} - X', Y', Z'\right). \tag{26}$$

By doing this, the particles then form a hemisphere with $\sqrt{X'^2 + Y'^2} < R_\mathrm{p}$. The total mass of this is taken to be $0.25m$. Most of these particles will be on weakly bound orbits when they are given the pericentre velocity appropriate to a zero energy orbit with pericentre at $(R_\mathrm{p}, 0, 0)$ in the Cartesian system. By following this procedure, we omit consideration of the ∼50 per cent of the disrupting star that will be unbound. However, this does not intersect the disc and so it does not play a significant role in our study. In addition, the number of bound particles that get transferred to the disc from the stream is increased. The initial velocity of a particle in the star is specified in the spherical polar coordinate system to be $\boldsymbol{v}_0 = \left(0, 0, v_{\phi,0}\right)$, where

$$v_{\phi,0} = \sqrt{\frac{2GM}{R_\mathrm{p}}}\sqrt{1 + 3\frac{R_\mathrm{g}}{R_\mathrm{p}}},$$

with $R_\mathrm{g} = \dfrac{GM}{c^2}$, R_g being the gravitational radius and c is the speed of light. Thus, neglecting the effect of black hole rotation which comes in at a higher order in $1/c$, each particle is given the pericentre velocity appropriate to a zero energy orbit passing through pericentre. Being for the most part weakly bound, they eventually return to the vicinity of pericentre in the form of a stream that persists till arbitrarily large times. We remark that the initial configuration of the star is not in hydrostatic equilibrium and so pressure forces might be expected to produce some artificial expansion. However, the initial ratio of sound speed to orbital velocity is $\sim 2 \times 10^{-3}$ which is very small. Thus, we anticipate the effects of pressure imbalance to be small until the stream first intersects itself. Tests we performed showed that until this stage, the motion of the stream was to a good approximation ballistic. At later times when the stream impacts disc material at larger radii $R/R_\mathrm{p} \sim 5$, the ratio of the width of the stream to the local radius is ∼0.1 indicating the operation of some viscous spreading.

4.2 Equation of state

4.2.1 Disc particles

For the disc, we adopt a locally isothermal equation of state for which the locally isothermal sound speed is given by $c_\mathrm{s} = \delta|\boldsymbol{v}_\perp|$. Here, $\delta = H/R$ is the disc semi-thickness with H being the disc scaleheight and we recall that $R = |\boldsymbol{R}|$ is the distance to the black hole. The component of the velocity vector of a particle that is perpendicular to $\boldsymbol{R}$ is $\boldsymbol{v}_\perp$. In order to determine $\boldsymbol{v}_\perp$, we set

$$\boldsymbol{v}_\perp = \boldsymbol{\omega} \times \boldsymbol{R}, \quad \text{with} \quad \boldsymbol{\omega} = \boldsymbol{R} \times \boldsymbol{v}/R^2, \quad \text{where} \tag{27}$$

$\boldsymbol{v}$ is the velocity vector of the particle and $\boldsymbol{\omega}$ its angular velocity vector. The direction of this is chosen so as to specify the required

disc orientation. The disc aspect ratio is chosen to be $\delta = 0.1$ for all simulations.

4.2.2 Stream particles

For the stream particles, we adopt an isothermal equation of state with a constant temperature of $T = 10^6$ K. The particles originating from the 'star' are evolved separately from the relaxed disc until just before the first particles return to periastron. After this stage, all the particles are allowed to interact. In so doing, stream particles are converted into disc particles. The criterion we adopted for specifying when this first occurred for a particular particle was that the ratio of binding energy to potential energy, calculated neglecting pressure and viscosity, should have become $<1/3$. At that point, the equation of state then switches from that for the stream to that for the disc, provided the sound speed is larger in the latter case. We remark that the small value of the ratio of the initial sound speed to orbital speed is found to result in the disc temperature always exceeding the initial stream temperature; accordingly, heating occurs when a particle originating in the stream becomes tagged as a disc particle and then only the equation of state changes.

The total number of particles involved in the simulations presented here is 4×10^5 with 50 per cent of these originating in the stream and 50 per cent in the disc. They have been checked by performing simulations with the particle number reduced by a factor of 4 which gave very similar results apart from in the very central regions with $R/R_\mathrm{p} = r_\mathrm{p} < 0.25$ where there are too few particles in the low-resolution runs.

4.3 A comparison of the disc inclination angle obtained from SPH simulations with semi-analytic results

In order to make a comparison between the semi-analytic approach developed above and the SPH simulations, we use the surface density Σ and the mass flux in the stream obtained from simulations as input background state variables to be used in equation (20). We determine a typical value of viscosity parameter α by comparing the dependence of the mass of the accretion disc as a function of time obtained from SPH simulations of a free accretion disc without the presence of the stream with an analytic model based on solution of the surface density evolution equation which incorporates an assumed value of α, the latter quantity being chosen to provide the best match. The analytic model is the same as described in Ivanov et al. (2015), with the adjustment that the kinematic viscosity is taken to be $\propto r_\mathrm{p}^{1/2}$. This procedure gives typical values of $\alpha \approx 0.1$, which is employed in our solution of equation (20) that yields the disc inclination angle.[6]

We consider two cases, both having $\delta = 0.1$, but different values of rotational parameter, namely $a = 1$ and 0.1. The results of the comparison are shown in Figs 6 and 7. In Fig. 6, we show the dependences of the disc inclination angle at the stream impact location on time; solid and dashed curves represent SPH results for $a = 1$ and 0.1, while dotted and dot–dashed curves are their respective counterparts obtained by solution of equation (20).[7] Note that all curves have been averaged over 100 data points corresponding to the time spans $10^3\Omega_\mathrm{p}^{-1}$ and $2 \times 10^3\Omega_\mathrm{p}^{-1}$ for $a = 1$ and 0.1, respectively, to remove numerical noise.

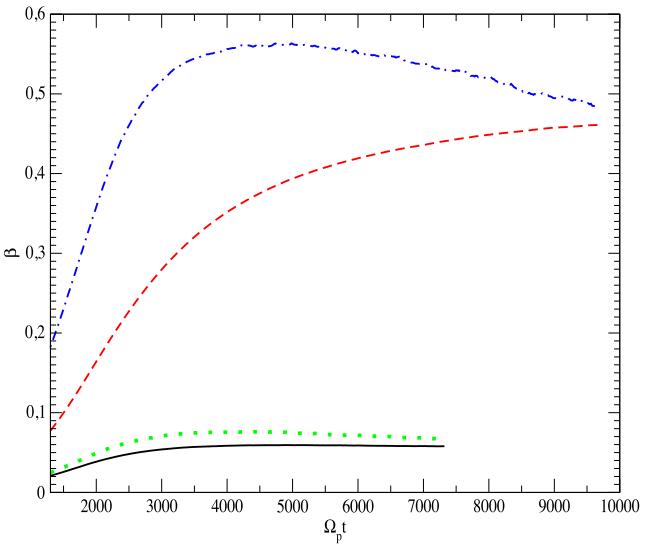

Figure 6. The dependence of the inclination angle β, in radians, at the stream impact position on time. See the text for a description of particular curves.

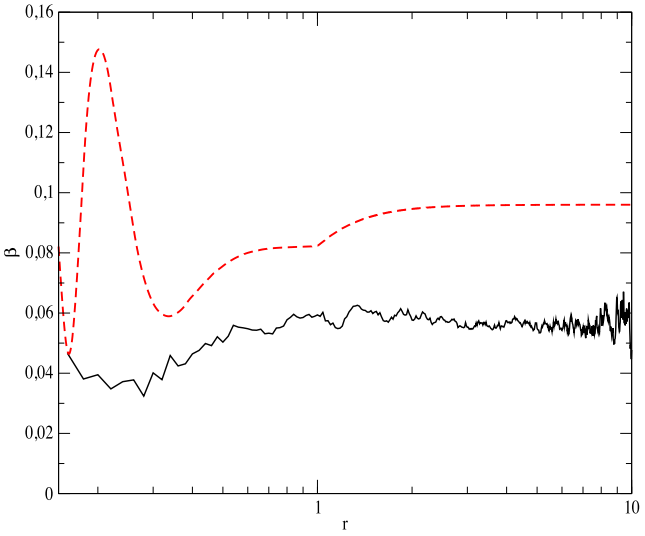

Figure 7. The inclination angle β, in radians, shown as a function of radial distance r_p for the case with $a = 1$ at time $t = 3500\Omega_\mathrm{p}^{-1}$. The solid curve is from an SPH simulation, while the dashed one is obtained by solution of equation (20), see the text for details.

We see that the analytic and SPH approaches are in agreement in finding that the case with $a = 1$ becomes quite closely aligned whereas the case with $a = 0.1$ maintains significant misalignment. Thus, we can expect that for discs with $\delta \sim 0.1$ and other parameters appropriate to the TDE we consider, significant alignments are to be expected for some systems. One can also see from Fig. 6 that

[6] We recall that the disc inclination angle β is defined as the angle between the direction of the Z-axis of our (X,Y,Z) Cartesian coordinate system, which coincides with the direction of the black hole rotation, and the unit vector perpendicular to the plane of a disc ring at a particular radius r. Also, we do not show behaviour at times prior to the beginning of stream–disc interaction, that is before the first stellar material returns to periastron.

[7] For the chosen values of α, δ and a, the parameters η and η_rel are approximately 0.6 and 0.9 for the $a = 1$ case, and 0.1, 0.4 for the $a = 0.1$ case.

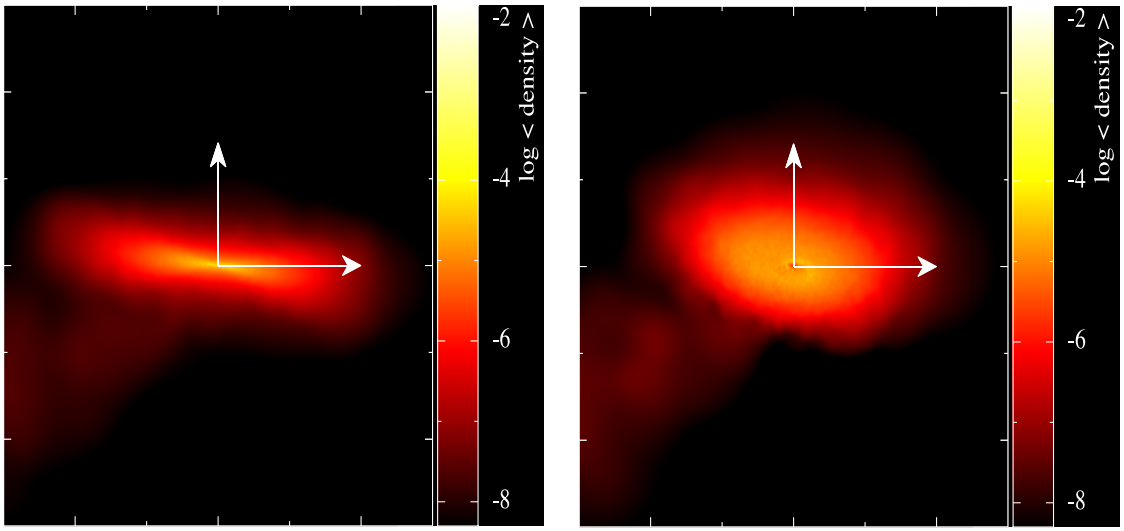

Figure 8. The disc and stream seen in projection at $t = 8000\Omega_{\rm p}^{-1}$. The case with $a = 1$ is illustrated in the left-hand panel and the case with $a = 0.01$ in the right-hand panel. In these plots, the long vertical axis is perpendicular to the line of sight and points in the direction of the black hole angular momentum. The orthogonal axis shown is the X-axis as defined in the text (see Section 2). The tick marks on the axes of the plots are separated by 10 dimensionless distance units. The colour scale indicates $\log \langle\rho\rangle$, with $\langle\rho\rangle$ being the projected density.

there is good agreement between the semi-analytic curves and those derived from SPH simulations corresponding to the case $a = 1$. The typical deviation is of the order of 20 per cent. When $a = 0.1$, there is a factor of 1.5–2 disagreement for times $<\approx 10^4\Omega_{\rm p}^{-1}$, which can perhaps be attributed to a slower relaxation of the twisted disc to a quasi-stationary configuration in this case. This is not unexpected as the time-scale associated with attaining alignment in the absence of the stream is expected to be longer for smaller values of the rotation parameter a. The disagreement becomes, however, quite small at later times with typical difference of the order of 5 per cent. To illustrate the appearance of the disc, we show projections of the density distribution at $t = 8000\Omega_{\rm p}^{-1}$ for $a = 1.0$ and 0.1 in Fig. 8. It will be seen that in agreement with the above discussion, the case with $a = 1.0$ is almost aligned with the black hole equatorial plane whereas there is significantly greater misalignment for $a = 0.1$.

In Fig. 7, we show the inclination angles as a function of radius at the time $t = 3500\Omega_{\rm p}^{-1}$. Solid curve and dashed curves illustrate results respectively obtained using the SPH method and by solving equation (20) for $a = 1$. One can see that the disc inclinations change at approximately the same radial scale. At radii $r_{\rm p} > 1$, the inclination angle stays approximately constant with its value being larger in the analytic approach by about 30–40 per cent.[8] This may be linked to the behaviour at small radii. For $\sim 0.4 < r_{\rm p} < \sim 1$, the inclination angle decreases towards black hole in both approaches. However, there is a qualitative difference in the behaviour of disc's tilt at smaller $r_{\rm p}$. While in the analytic approach the inclination angle oscillates with a rather large amplitude, the numerical simulations give a much more moderate evolution. This difference can be attributed to an insufficient number of SPH particles to fully resolve the oscillations of the disc tilt. In our case, $N = 4 \times 10^5$. We remark that a specially dedicated study shows that the number of particles required to achieve this should be an order of magnitude larger (see Nealon, Price & Nixon 2015).

[8] Let us note that numerical grid-based magnetohydrodynamic (MHD) calculations also give typical values of the disc tilt smaller than semi-analytic ones by a factor of 2 (see Zhuravlev et al. 2014).

To summarize, there is full qualitative agreement between the two approaches apart from the issue of the disc tilt behaviour at small radii, which is not important for our purposes. For the significant quantities and/or values of parameters, there is quite good quantitative agreement. This validates the use of our analytic approach for much more realistic backgrounds evolving over much longer times $\sim 10^5$ orbital periods at periastron provided by our grid-based 1D finite difference numerical simulations (see Section 5 below). It is impracticable to carry out SPH simulations for such long times.

5 GRID-BASED CALCULATIONS OF THERMALLY UNSTABLE DISCS

We have performed grid-based simulations of an accretion disc supplied by a stream produced by a tidally disrupted star. The expected accretion rate is sufficiently large that the Eddington limit is exceeded, radiation pressure becomes important and the disc undergoes thermal instability. This instability produces transitions between high and low states that in some circumstances can move as propagating fronts. When the accretion rate is approximately steady in the mean, cyclic behaviour may occur in which there is alternation between high and low states.

The formalism is similar in concept to that of Szuszkiewicz & Miller (1998), who considered the evolution of thermal instabilities in accretion discs for which radiation pressure plays a significant role. However, it is adapted to conditions around a $10^6\,{\rm M}_\odot$ black hole rather a $10\,{\rm M}_\odot$ black hole that they studied. In addition, radiative transfer in the radial direction and mass input from an accretion stream produced by tidal disruption are considered.

Furthermore, our simulations have been performed with NIRVANA which is a three-dimensional MHD code that has been described in e.g. Ziegler & Yorke (1997). For the grid-based calculations performed here, the magnetic field is set to zero and the code is restricted to operate in one dimension. For convenience, we retain spherical polar coordinates restricted to the plane $\theta = \pi/2$ and assume that the system is independent of the azimuthal coordinate. The sole independent spatial coordinate, being the radius, R, can then be regarded as a cylindrical coordinate. Note that we solve

the governing equations in Eulerian form and so our procedure differs markedly from the one-dimensional Lagrangian approach implemented by Szuszkiewicz & Miller (1998).

5.1 Basic equations

The basic equations are those of mass, momentum and energy conservation appropriate to a mixture of gas and radiation. In a non-rotating frame with origin at the location of the black hole, these take the form

$$\frac{\partial \Sigma}{\partial t} + \nabla \cdot (\Sigma \boldsymbol{v}) = S_m \,, \tag{28}$$

$$\Sigma \left(\frac{\partial \boldsymbol{v}}{\partial t} + \boldsymbol{v} \cdot \nabla \boldsymbol{v} \right) = -\nabla \Pi - \Sigma \nabla \Phi + \boldsymbol{f}_v, \tag{29}$$

$$\frac{\partial E}{\partial t} + \nabla \cdot (E \boldsymbol{v}) = -\Pi \nabla \cdot (\boldsymbol{v}) + \epsilon_v - 2F_+ - \nabla \cdot (2HF\hat{R}) + S_{\rm E}. \tag{30}$$

Here, $\boldsymbol{v} = V_{\rm R}\hat{\boldsymbol{R}}$ is the velocity, with $\hat{\boldsymbol{R}}$ being the unit vector in the radial direction, Π is the vertically integrated pressure and E is the vertically integrated internal energy per unit volume. The viscous force per unit area is $\boldsymbol{f}_v$, the rate of energy input per unit area due to viscous dissipation is ϵ_v and the radiation flux per unit area leaving one side of the disc is F_+. The factor of 2 multiplying this quantity accounts for the two sides of the disc. The radiative flux in the radial direction is

$$F = -\frac{c}{\kappa\rho}\frac{\partial (a_R T^4/3)}{\partial R}. \tag{31}$$

The opacity is κ and a_R is the Stefan–Boltzmann constant. The mass input rate per unit area from the stream is S_m, which is discussed further in Section 5.5 below, and the rate of excess thermal energy input per unit area associated with this is $S_{\rm E}$. For these studies, we adopt the Paczyński–Wiita potential such that $\Phi = -GM/(R - 2R_{\rm g})$. Here, as elsewhere, the self-gravity of the gas is neglected.

5.2 Equation of state

The two state variables we use to characterize the mixture of gas and radiation are Σ and E. These are related to the mid-plane density and internal energy density through $\Sigma = 2H\rho$ and $E = 2HU$, respectively, where H is an effective semi-thickness. We make the assumption that this is the same for both quantities and also that $\Pi = 2HP$, where P is the mid-plane pressure. Then from the expressions for P and U in terms of ρ and T given by

$$P = (\mathcal{R}/\mu)\rho T + a_R T^4/3 \quad \text{and} \quad U = (3\mathcal{R}/2\mu)\rho T + a_R T^4, \tag{32}$$

on the disc mid-plane we obtain

$$\Pi = (\mathcal{R}/\mu)\Sigma T + 2Ha_R T^4/3 \quad \text{and}$$

$$E = (3\mathcal{R}/2\mu)\Sigma T + 2Ha_R T^4. \tag{33}$$

Here the mean molecular weight is μ and $\mathcal{R}$ is the gas constant. Once H is related to E and Σ, all of the local state variables can be found. For example, the temperature is found by solving the quartic equation obtained from the second expression in equation (33). We adopted the expression

$$H = \sqrt{\frac{2\sqrt{2}E}{3\Sigma\Omega^2}} \tag{34}$$

for the semi-thickness H. Regarding this, we recall that from vertical hydrostatic we get the conventional estimate

$$H = \sqrt{2P/(\rho\Omega^2)}. \tag{35}$$

Noting that in the gas pressure-dominated limit, we have $P/\rho = 2E/(3\Sigma)$ and in the radiation-dominated limit we have $P/\rho = E/(3\Sigma)$, the value of H obtained from equation (34) differs from equation (35) by at most $2^{1/4}$. As this is within the uncertainties inherent in carrying out the vertically averaging procedure, we adopt equation (34). For the calculations reported here, the mass fraction in hydrogen was taken to be 0.7 and $\mu = 0.615$.

5.3 Radiative cooling and viscosity

The emergent radiation flux is given by

$$F_+ = \frac{2a_R c T^4}{(3\kappa\Sigma + 4/3)}. \tag{36}$$

Equation (36) is obtained by writing $F_+ = a_R c T_{\rm eff}^4/4$, where $T_{\rm eff}$ is the effective temperature. Using the Eddington approximation to relate T and $T_{\rm eff}$ then gives equation (36). We remark that $\kappa\Sigma/2$ is the optical depth of the mid-plane. For the model considered here, we assume that the opacity is due to electron scattering and accordingly is constant.

Viscosity is incorporated through adopting the standard α parametrization of Shakura & Sunyaev (1973). Using this, the kinematic viscosity is given by

$$\nu = \alpha P/(R\rho|{\rm d}\Omega/{\rm d}R|) \;\; \text{leading to} \;\; \langle\nu\rangle = \alpha\Pi/(R\Sigma|{\rm d}\Omega/{\rm d}R|), \tag{37}$$

where $\langle\nu\rangle$ is the density-weighted vertically averaged viscosity.

When the disc becomes thermally unstable, it can become very thick, with H/R driven to values exceeding unity. Our formalism then becomes inappropriate. It is also likely that some of the available energy goes into driving an outflow rather than mid-plane heating. Accordingly, we have limited the heat production rate when the disc becomes thick. For the runs considered, we applied a reduction factor $(1 - (H/R))^2$ to the heating rate. Although this quenching is ad hoc, it limits the growth of H/R of the disc region modelled, but otherwise does not affect the qualitative form of the results.

5.4 Computational domain and boundary conditions

Simulations were performed over the radial domain $[R_{\rm in}, R_{\rm out}]$ with $R_{\rm in} = 3.0388 \times 10^{12}$ cm and $R_{\rm out} = 1.484\,012 \times 10^{13}$ cm. We have employed $N_{\rm g} = 768$ equally spaced grid points and checked convergence using twice as many ($N_{\rm g} = 1536$).

At both radial boundaries, we employ a limited outflow condition. This is the same as the standard outflow condition but with the additional feature that the magnitude of the outflow velocity is limited to be less than or equal to $3\langle\nu\rangle/(2R_{\rm out})$. These velocities are characteristic of the inflow velocity driven by viscosity and will remain small if the disc remains thin. However, they can become moderately large without causing a major pile-up of mass when the disc becomes thick, if α is not too small. Thus, advective transport can arise when the disc becomes thermally unstable.

5.5 Input from the stream

For a star of $1\,{\rm M}_\odot$, the pericentre distance for a penetration factor $B_{\rm p}$ is given by $R_{\rm p} = 7 \times 10^{12}(M/(10^6\,{\rm M}_\odot)^{1/3}/B_{\rm p}$ (see Section 2.1).

For our simulations, we take $M = 10^6\,\mathrm{M}_\odot$ and $B_\mathrm{p} = 14/9$. Then the pericentre distance is 4.5×10^{12} cm and the minimum return time is $P_\mathrm{min} = 3.5 \times 10^6 B_\mathrm{p}^{-3}\,\mathrm{s} = 9.30 \times 10^5$ s.

We adopt the following simplified prescription for the accretion rate $\dot{M}_\mathrm{S}$ from the stream generated by the tidally disrupted star. Setting $t = 0$ to be the time of pericentre passage, we take $\dot{M}_\mathrm{S} = 0$ for $t < P_\mathrm{min}$. For $t > P_\mathrm{min}$, we set $\dot{M}_\mathrm{S} = 7.17 \times 10^{26}(t/P_\mathrm{min})^{-5/3}\,\mathrm{g\,s^{-1}}$. Thus, we assume a tail off $\propto t^{-5/3}$ (Lodato et al 2009 and references therein) and a total mass to be accreted of $0.5\,\mathrm{M}_\odot$. This mass accretion rate is input uniformly over eight grid cells centred on the circularization radius $R_\mathrm{S} = 2R_\mathrm{p}$ at the lowest resolution. For higher resolutions, the number of grid cells used is proportional to the resolution. This procedure determines S_m. We remark that this simplified model assumes that the stream has a high enough density that it is able to penetrate any intervening disc material in order to reach the circularization radius, avoiding prior significant angular momentum exchange. This scenario may require modification when the disc becomes very thick at late times when the accretion rate is small. However, for simplicity, we adopt it throughout.

When mass from the stream enters the disc, energy is dissipated. Assuming that the plane of the stream is only slightly inclined to that of the disc, the kinetic energy per unit mass associated with radial motion available to be dissipated is $GM/(2R_\mathrm{S})$. Depending on details of the circularization process, a part of this is radiated away directly and a part is converted to excess internal energy of the disc. This energy is input along with and in the same way as the mass input in this way S_E is determined. For simplicity, we have assumed this fraction to be $f_\mathrm{st} = 50$ per cent for the simulations presented here. However, we have also run cases with this input reduced by more than an order of magnitude. We have found that this does not change the qualitative form of the results significantly as the internal energy provided by dissipation of stream kinetic energy ultimately never dominates that arising from viscous dissipation throughout the disc.

5.6 Initial disc

The steam commences to input mass at $t = P_\mathrm{min}$ into an initial disc. This was specified to have a low mass of $0.011\,\mathrm{M}_\odot$ as compared to the total to be input from the stream. The state variables were chosen such that $\beta = 0.5$ was constant with $\rho \propto R^{-3}$ for $R < 7.572 \times 10^{13}$ and $\rho \propto R^{-1}$ for $R < 7.572 \times 10^{13}$. With this choice, $\Sigma \propto R^{-2}$ for $R < 7.572 \times 10^{13}$ and $\Sigma \propto R^{1/3}$ for $R > 7.572 \times 10^{13}$. We remark that as after a short time the simulation is dominated by the mass input from the stream, which occurs at a rate implying that the Eddington limit is exceeded (see Section 6 below), results are not expected to be affected by the choice of initial disc structure. Profiles are rapidly modified by outward propagating transition fronts. Thus, reducing the initial value of β by a factor of 2 has no significant effect.

5.7 Simulation of a flat disc

Simulation results for model A with $\alpha = 0.3$ are illustrated in Fig. 9. The uppermost panels show the evolution of the first outwardly propagating transition front. The forms of the surface density and the semi-thickness are plotted. A front is seen to have formed after a time given by $(t - P_\mathrm{min})/P_\mathrm{min} = 0.216$ and reaches the outer boundary after a time given by $(t - P_\mathrm{min})/P_\mathrm{min} = 0.865$. At this stage, the disc attains a high state with $H/R \sim 1$ in the inner and outer parts, being somewhat smaller in the central regions. After a time given by $(t - P_\mathrm{min})/P_\mathrm{min} = 37.83$, an inwardly propagating front is seen in the outer parts of the disc. Its evolution is shown in the second row of panels of Fig. 9. After a time approximately given by $(t - P_\mathrm{min})/P_\mathrm{min} = 47$, this stalls at a radius $R \sim 5 \times 10^{13}$ cm and the evolution enters a quasi-steady phase with the outer disc in a low state. The total mass content of the disc and the accretion rate through the boundary are shown in the lowermost panels of Fig. 9. It will be seen that during the time the disc is in a high state between these upward and downward transitions, around $0.1\,\mathrm{M}_\odot$ is accreted through the centre by means of a strong advective flow. At later times a series of cycles takes place in which parts of the disc alternate between high and low states. The presence of these can be seen through the behaviour of the mass accretion rate into the central regions at late times where several distinct oscillations can be seen. Before this behaviour is noticeable, there are several outbursts for which the whole disc is again in a high state. At increasingly late times, the outbursts become progressively more confined in the central parts of the disc with the outer parts remaining in a low state. This is a naturally expected outcome as the mass input rate from the stream declines towards zero. The third row of panels illustrate the evolution of the outburst that occurs for $18.9126.15 < (t - P_\mathrm{min})/P_\mathrm{min} < 128.15$. During this outburst, the accretion rate into the centre is affected and the outer parts of the disc remain in a low state throughout. Also during the heating phase of the disc, there are two regions in a high state separated by a region in a low state.

Simulation results for model B with $\alpha = 0.1$ are illustrated in Fig. 10. The uppermost panels again how the evolution of the first outwardly propagating transition front. In this case, the front is seen to have formed after a time given by $(t - P_\mathrm{min})/P_\mathrm{min} = 0.649$ and reaches the outer boundary after a time given by $(t - P_\mathrm{min})/P_\mathrm{min} = 2.594$. It is accordingly about a factor of 2 slower than for model A. The entire disc again goes into a high state with $H/R \sim 1$. However, its duration is somewhat shorter in this case. After a time given by $(t - P_\mathrm{min})/P_\mathrm{min} = 29.186$, an inwardly propagating front can be seen in the outer parts of the disc. Its evolution is shown in the second row of panels of Fig. 10. After a time given approximately by $(t - P_\mathrm{min})/P_\mathrm{min} = 44$, this stalls at a radius $R \sim 4 \times 10^{13}$ cm and the evolution again enters a quasi-steady phase with the outer disc in a low state. The total mass content of the disc and the accretion rate through the boundary shown in the lowermost panels of Fig. 10 indicate that when the disc is in a high state between these transitions, around $0.05\,\mathrm{M}_\odot$ is accreted through the centre being about half of that found for model A. As for model A, a sequence of cyclic heating and cooling events occurs. However, these are more confined to the outer disc and tend to involve smaller radial scales, which decrease as time progresses. The third row of panels illustrate the evolution of the outburst that occurs for $45.131 < (t - P_\mathrm{min})/P_\mathrm{min} < 54.319$. In this case, although the region of the disc closest to the outer boundary remains in a low state, the heating commences in the outer part of the disc converting a section into a high state with very little effect on the innermost regions. During the cooling phase, the high-state outer region collapses while the innermost high-state region retreats inwards. Continuation of this calculation, as for model A, results in outbursts that become progressively more confined in the central parts of the disc as the accretion rate reduces with the outer parts remaining in a low state but with small-scale fluctuations.

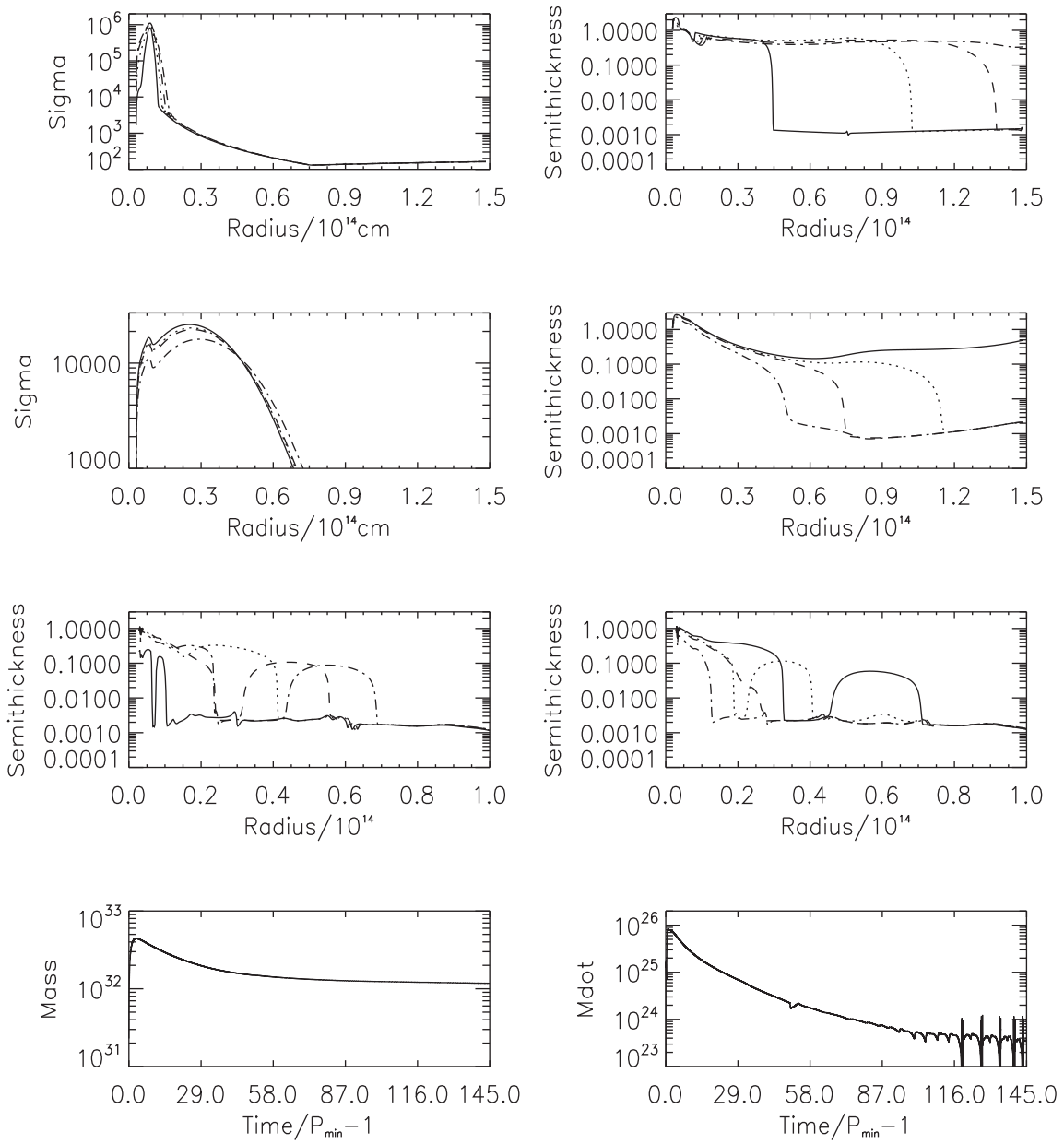

Figure 9. Simulation results for model A with $\alpha = 0.3$ are shown. The uppermost panels show the evolution of the first outwardly propagating transition front. The left-hand panel shows the surface density and the right-hand panel the semi-thickness. Their functional forms are given at times expressed in the form $(t - P_{\rm min})/P_{\rm min}$ of 0.216 (solid curve), 0.432 (dotted curve), 0.649 (dashed curve) and 0.865 (dot–dashed curve). The second row of panels show the evolution of the first inwardly propagating transition front. The left-hand panel shows the surface density and the right-hand panel the semi-thickness. Their functional forms are given at times expressed in the form $(t - P_{\rm min})/P_{\rm min}$ of, 37.83, (solid curve) 40.00, (dotted curve) 41.08 (dashed curve) and 47.56 (dot–dashed curve). The third row of panels show the evolution of a later outburst. The left-hand panel shows the semi-thickness during the heating phase and the right-hand panel the semi-thickness during the cooling phase. Their functional forms are given at times expressed in the form $(t - P_{\rm min})/P_{\rm min}$ of 118.91 (solid curve), 120.10 (dotted curve), 121.29 (dashed curve) and 122.53 (dot–dashed curve) for the left-hand panel and of 122.96 (solid curve), 123.72 (dotted curve), 124.91 (dashed curve) and 126.15 (dot–dashed curve) for the right-hand panel. The lowermost left-hand panel shows the mass in the disc in grams as a function of time. The lowermost right-hand panel shows the accretion rate into the central part of the disc in g s^{-1} as a function of time.

5.8 The evolution of the inclination angle for background disc models obtained from the grid-based simulations

In order to find the evolution of twist and tilt angles as a function of time, we numerically integrate equation (20) using the grid-based models described above to specify the dependence of the semi-thickness, δ, and surface density, Σ, on time, for model A with $\alpha = 0.3$ and model B with $\alpha = 0.1$ (see Table 2). Other disc parameters are fixed as indicated above. Note that the surface density enters equation (20) implicitly through the quantities, σ, defined through equation (22), and $\xi = \delta^2 \Sigma r^{1/2}$. To find the mass flux in the stream, we use equation (5) when $t > P_{\rm min}$ and assume that $\dot{M}_{\rm S} = 0$ at earlier times. The outer radius of the integration domain was fixed to be $r_{\rm out} = 18$, while the inner radius was taken to be $r_{\rm in} = 0.25$ for the cases where the inclination angle exponentially grows for $r < 1$ and $r_{\rm in} = 0.04$ for the cases where it oscillates at small values of r. We consider a range of values for the black hole rotation parameter

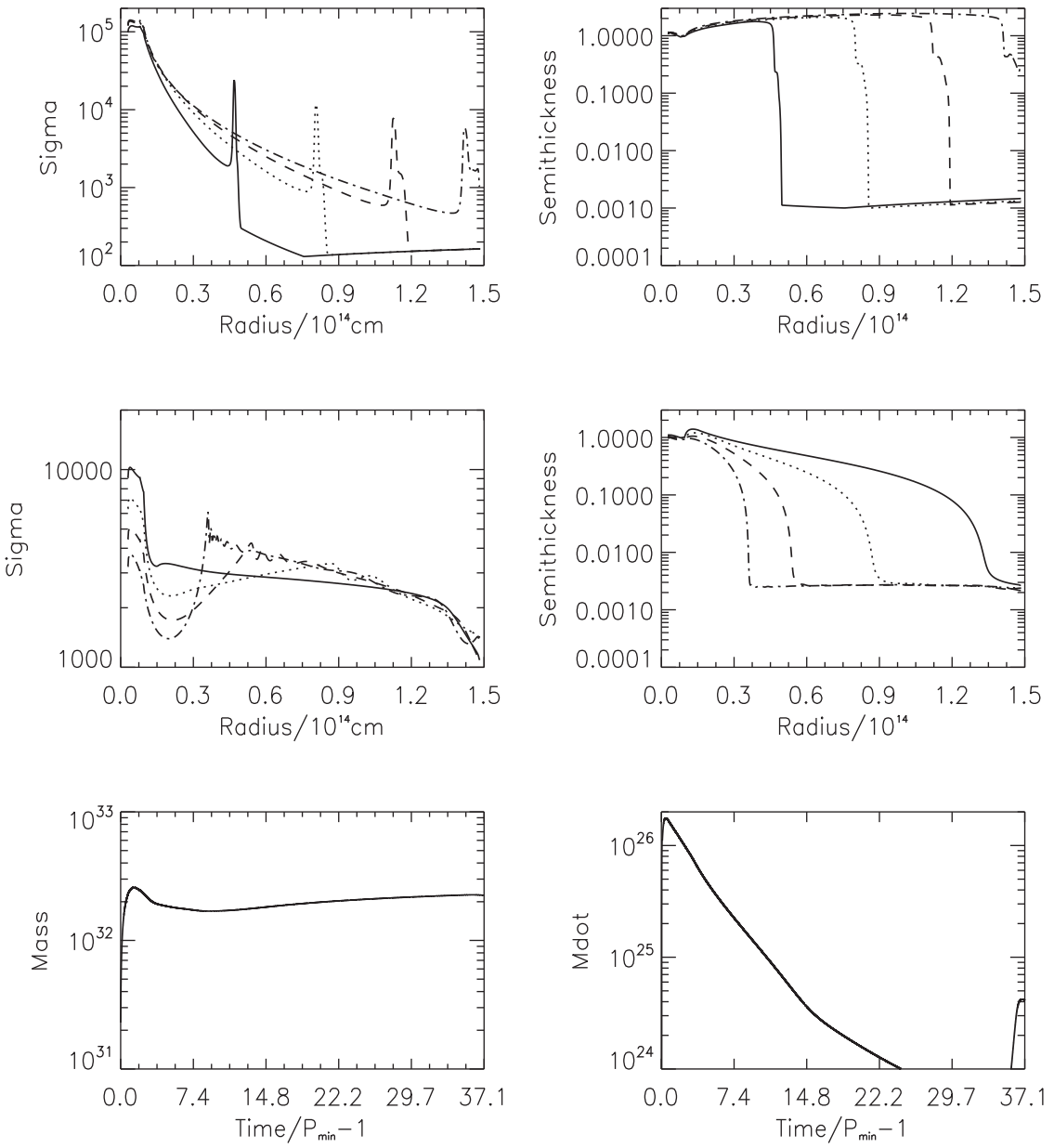

Figure 10. Simulation results for model B with $\alpha = 0.1$ are shown. The uppermost panels show the evolution of the first outwardly propagating transition front. The left-hand panel shows the surface density and the right-hand panel the semi-thickness. Their functional forms are given at times expressed in the form $(t - P_{\rm min})/P_{\rm min}$ of 0.649 (solid curve), 1.297 (dotted curve), 1.946 (dashed curve) and 2.594 (dot–dashed curve). The second row of panels show the evolution of the first inwardly propagating transition front. The left-hand panel shows the surface density and the right-hand panel the semi-thickness. Their functional forms are given at times expressed in the form $(t - P_{\rm min})/P_{\rm min}$ of 29.186 (solid curve), 34.051 (dotted curve), 38.915 (dashed curve) and 44.320 (dot–dashed curve). The third row of panels show the evolution of a later outburst. The left-hand panel shows the semi-thickness during the heating phase and the right-hand panel the semi-thickness during the cooling phase. Their functional forms are given at times expressed in the form $(t - P_{\rm min})/P_{\rm min}$ of 45.131 (solid curve), 45.779 (dotted curve), 46.158 (dashed curve) and 46.482 (dot–dashed curve) for the left-hand panel and of 47.563 (solid curve), 49.725 (dotted curve), 51.887 (dashed curve) and 54.319 (dot–dashed curve) for the right-hand panel. The lowermost left-hand panel shows the mass in the disc in grams as a function of time. The lowermost right-hand panel shows the accretion rate into the central part of the disc in g s^{-1} as a function of time.

a and both prograde and retrograde rotation. Note that although the background models were obtained with this set to zero, they are not expected to have a significant dependence on it. However, this is not the case for the disc inclination when the disc suffers a misaligning perturbation.

We show the value of the inclination angle β in units of the stream inclination β_* as a function of time $\tau = t/P_{\rm min}$ in Figs 11 and 12, respectively, for models A and B.

Table 2. Parameters of models for which results are described in the text.

Model	α	$f_{\rm st}$
A	0.3	1.0
B	0.1	1.0

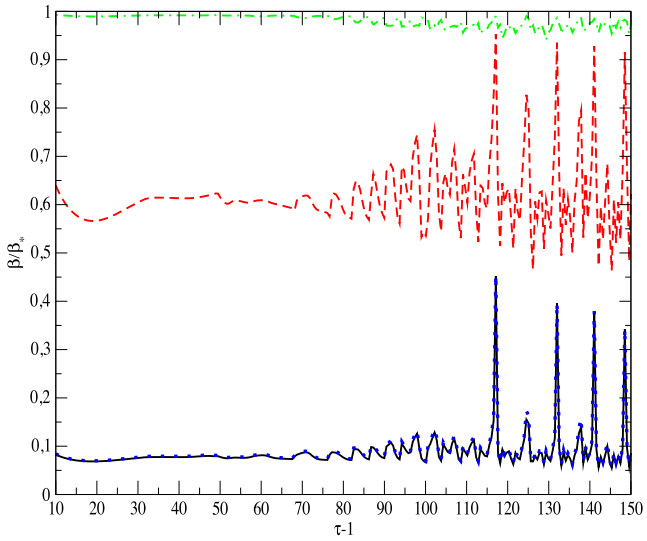

Figure 11. The value of inclination angle β at the stream impact position $r = 1$ as a function of time $\tau = t/P_{\rm min}$ shown for the grid-based model with $\alpha = 0.3$. See the text for a description of different particular curves.

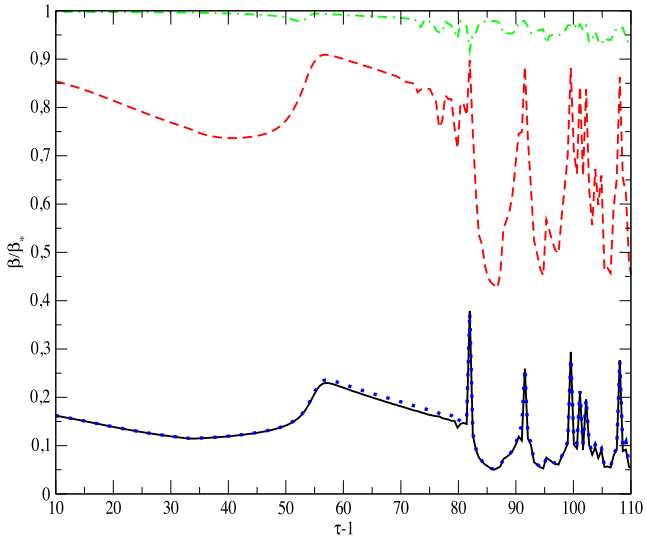

Figure 12. The value of inclination angle β at the stream impact position $r = 1$ as a function of time $\tau = t/P_{\rm min}$ shown for the grid-based model, B, with $\alpha = 0.1$. See the text for a description of different particular curves.

In Figs 11 and 12, solid, dashed and dot–dashed lines illustrate calculations for prograde rotation of the black hole with $a = 1$, 0.1 and 0.01, respectively. From these results, it is apparent that smaller black hole rotations lead to larger disc inclinations, as expected. In addition, the time-averaged values of the inclination for $a = 0.1$ and 1 are similar in magnitude to those found for the SPH simulations of a disc with $\delta \sim 0.1$ throughout as discussed in Section 4. The dotted curves illustrate the case of retrograde rotation with $a = -1$. Since results found for retrograde rotation with a smaller absolute value of a practically coincide with those obtained for its prograde counterpart, they are not shown.

The results illustrated in Figs 11 and 12 indicate that values of the scaled inclination are quite substantial for our models at all times, being of the order of 0.1 for $a = 1$ and larger for smaller values of rotational parameter. The high-state super-Eddington regime of accretion corresponds to $\tau = t/P_{\rm min} < \tau_{\rm crit} \approx 80$–$100$. When $\tau > \tau_{\rm crit}$,

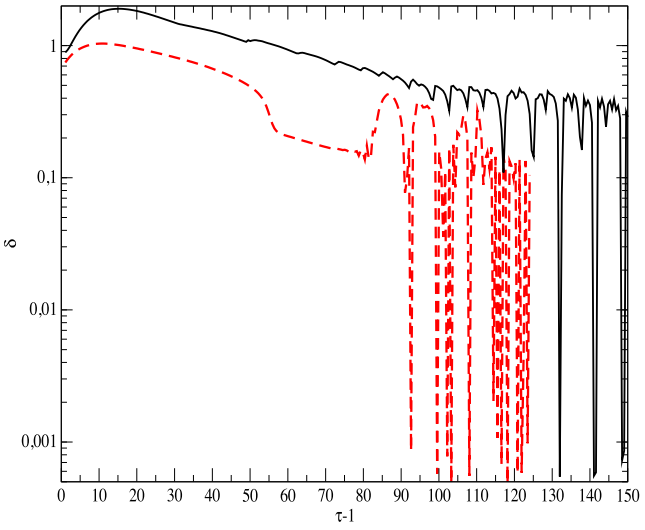

Figure 13. Dependences of $\delta(R = 0.5R_{\rm S})$ on time are shown. Solid and dashed lines correspond to models A and B, respectively.

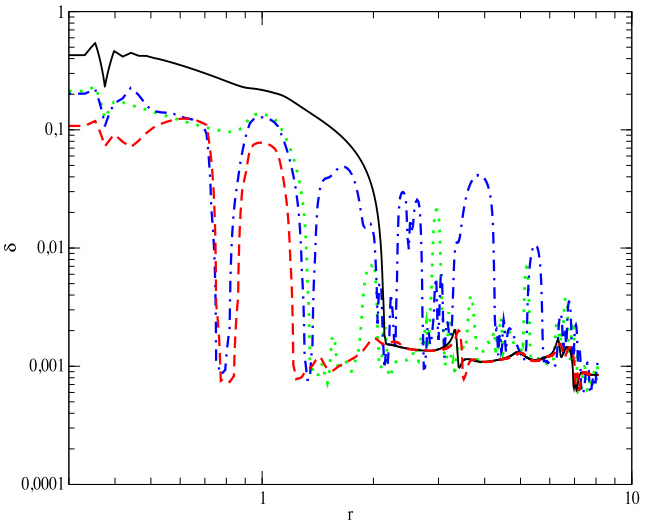

Figure 14. The dependence of the disc semi-thickness δ on radius r for different disc models at different times, see the text for description of the different curves.

a transition to the low state occurs, but, since there is a continuing supply of mass from the stream and radiation pressure is important, the condition for the development of thermal instability will become satisfied with the result that the disc undergoes a sequence of transitions between high and low states. The inclination angle changes quite dramatically in course of these transitions being of the order of the maximal values at low states and dropping to values of the order of $(0.05-0.1)\beta_*$ during the intermittent high states.

These sharp changes in disc inclination are related to sharp changes of the aspect ratio δ during these transitions. In order to illustrate this, we show the dependence of $\delta(R = 0.5R_{\rm S})$ on time in Fig. 13. Solid and dashed lines represent models A and B, respectively. One can see from this figure that the inclination angle and disc semi-thickness experience strong variations at the same time.

We show the functional form of δ and β with radius in models A and B immediately before and after the first transition from a high to a low state. In Figs 14 and 15, solid and dashed curves are for model A at $\tau = 115.5$ and 117, while the dotted and dot–dashed

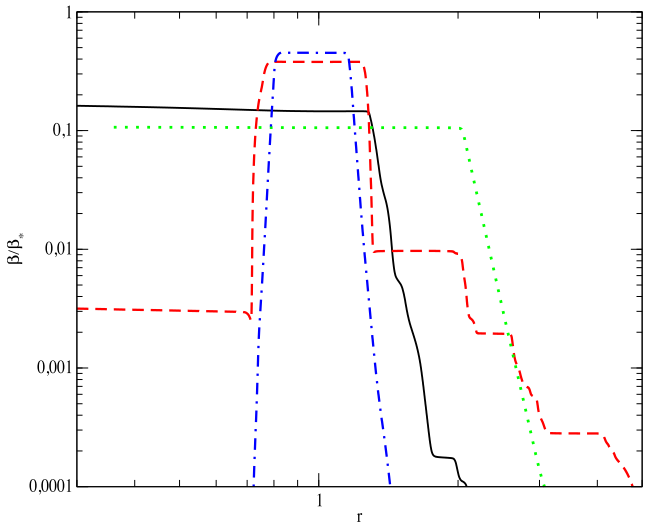

Figure 15. Same as Fig. 14, but the form of the inclination angle β is shown, see the text for description of different lines.

curves are for model B at $\tau = 80.4$ and 82. Solid and dotted curves apply during the high state, while dashed and dot–dashed curves are for the low state. It is seen that there is a clear relationship between a sharp decrease of δ in the vicinity of $r \sim 1$ and a corresponding growth of inclination angle. Note that this is more prominent for model A. Also note that even in the low state δ is much larger that its 'low' value of 10^{-3} very close to $r = 1$. This is related to heating the disc by the stream.

6 ANALYTIC ESTIMATES FOR $\tau_{\rm crit}$ AND THE POSSIBILITY OF LARGE VALUES OF THE DISC INCLINATION DURING THE TRANSITION TO A 'LOW STATE'

In our numerical work, we have considered disc models for only a small range of parameters characterizing them. Therefore, it is important to obtain estimates of the transition time $\tau_{\rm crit}$ and maximal values of β during these transitions, which can be applied to models characterized by a wider range of parameters such as any value of $\alpha < 1$.

A crude estimate of the transition time $\tau_{\rm crit}$, at which a major part of the disc first transitions from a high to low state, can be obtained from the following simple considerations (see also Shen & Matzner 2014 and references therein). During the high state, energy dissipated through the action of viscosity per unit time in a disc annulus centred at radius R and of unit width is mainly advected towards black hole. It is accordingly larger than the amount of energy radiated away by this annulus. The rate of dissipation of energy per unit radial width, $\dot{E}_{\rm diss}$, can be related to the mass flux $\dot{M}$ through $\dot{E}_{\rm diss} = 3GM/(2R^2)\dot{M}$ (e.g. Abramowicz et al. 1988), while the rate of radiation of energy from the annulus is equal to the flux, F_+, multiplied by $4\pi R$ to take into account both disc surfaces. In the advective stage, we therefore have

$$\dot{E}_{\rm diss} = \frac{3GM}{2R^2}\dot{M} > 4\pi R F_+, \tag{38}$$

where we assume that angular frequency of the disc material is approximately Keplerian.

As discussed above, in the optically thick limit, we specify $F_+ = 2cP_{\rm r}/(\kappa\Sigma)$, where κ is the Thomson opacity and $P_{\rm r}$ is radiation pressure. We also use the vertical component of the hydrostatic equilibrium equation which leads to $P = GM/(2^{5/2}R^3)\Sigma H$, where P is the total pressure and we recall that $H = \delta R$.

We now assume that $P \approx P_{\rm r}$ and express the mass flux in terms of the Eddington value $\dot{M}_{\rm E} = 4\pi GM/(c\kappa)$ as $\dot{M} = \dot{M}_{\rm E}\dot{m}$ which introduces a dimensionless accretion rate $\dot{m}$. We then substitute the resulting expression in equation (38) and use the expressions for radiation flux and the total pressure given above to obtain

$$\dot{m} > \frac{\delta}{3\sqrt{2}}\frac{R}{R_{\rm g}}, \tag{39}$$

in order that advective cooling overcomes radiative cooling. Now we assume that $R \sim R_{\rm S}$, use the definition of $B_{\rm S}$ and equation (1) to get

$$\dot{m} > 11\delta M_6^{-2/3}/B_{\rm S}. \tag{40}$$

Note that this implies that a thick advective disc with $M_6 \sim 1$ and $B_{\rm S} \sim 1$ will always be accreting at a rate that implies that the Eddington limit is exceeded.

We further make the assumption that the accretion rate may be taken to be that provided by the stream so that $\dot{M} \sim \dot{M}_{\rm S}$.[9] We recall that $\dot{M}_{\rm E} \approx 1.7 \times 10^{23} M_6\,{\rm g\,s^{-1}}$ and use equation (5) to find that in order that the inequality (40) to be broken we should require that

$$\tau < \tau_{\rm crit} \sim 20\left(\frac{B_{\rm S}B_{\rm p}^3}{\delta}\right)^{3/5} M_6^{-1/5}. \tag{41}$$

Note that the parameters used in our simulation, $\delta \sim 0.5$, $B_{\rm S} = 0.5B_{\rm p} \approx 1.55$ and $M_6 = 1$ in equation (41) give $\tau_{\rm crit} \approx 60$, which is somewhat smaller than the numerically obtained value $\tau_{\rm crit} \approx 80$–100. This, however, is well within an expected uncertainty based on the approximations leading to equation (41). Also, disc's semi-thickness δ is smaller than 0.5 in the end of high state, which could lead to larger $\tau_{\rm crit}$ in a more accurate model. It is instructive to rewrite equation (41) in physical units. With the help of equation (4), we obtain

$$t_{\rm crit} \equiv P_{\rm min}\tau_{\rm crit} \approx 2(B_{\rm S}/\delta)^{3/5}B_{\rm p}^{-6/5}M_6^{7/10}\,{\rm yr}. \tag{42}$$

Thus, the expected time to the beginning of the transition to the low state, and, accordingly, the most prominent deformation of the disc shape due to the stream influence is of the order of a few months to years.

6.1 Conditions for misalignment

Now let us consider conditions under which the inclination angle β can attain values of the order of β_* at $\tau_{\rm crit}$. As we have seen in Section 3 and Appendix A, the important quantities determining the degree of misalignment are the ratio of the alignment radius to $R_{\rm S}$, η or $\eta_{\rm rel}$ together with σ and $\sigma_{\rm rel}$, respectively. The latter quantities measure the ratio of the warp diffusion time or propagation time to the accretion time. Accordingly, a large value for them, coupled with small or modest values for the ratio of the alignment radius to $R_{\rm S}$, favours misalignment (see Appendix A).

We begin by evaluating typical values of the parameter σ given by equation (22) and accordingly, of the parameter $\sigma_{\rm rel}$ in the two states, see equation (A14). In order to do this, we assume that during the high state an approximate equilibrium between mass flow in the stream and disc is maintained with the mass flow in the disc being

[9] Note that this assumption may not be valid when α is small; however, we have checked that it holds for the considered values of α.

close to the typical value $\dot{M} = 3\pi\nu\Sigma$. Equating this expression to $\dot{M}_{\rm S}$ and using equations (5) and (13), we find

$$\tilde{\Sigma}_{\rm high} \sim \frac{1}{3}\tau^{-5/3} / \left(\alpha\delta_{\rm high}^2 P_{\rm min}\Omega_{\rm S}\right), \quad (43)$$

where $\delta_{\rm high} \sim 1$ is a typical disc semi-thickness during the high state.

When $\tau \sim \tau_{\rm min}$, δ drops to its low value $\delta_{\rm low} \sim 10^{-3}$. At this stage, the equilibrium between mass flows in the disc stream is no longer possible, since a typical viscous relaxation time in the disc becomes very long, and the disc is not able to effectively transfer the mass supplied by the stream from the stream impact region. Therefore, there is an accumulation of mass near $R \sim R_{\rm S}$. However, at the beginning of this stage, the mass accumulated in this region will be rather small and we can roughly estimate the surface density at this time to be equal to its value during the preceding high state. Substituting this value which may be obtained from equation (43) into equation (22) and remembering that $\delta = \delta_{\rm low}$, we get an estimate for the value of σ in the high state as

$$\sigma_{\rm max} \sim 6\left(\frac{\delta_{\rm high}}{\delta_{\rm low}}\right)^2 \alpha^2 \approx 13.5 q\alpha_{-2}^2, \quad (44)$$

where $\alpha_{-2} = \alpha/10^{-2}$, and $q = (\delta_{\rm high}/(150\delta_{\rm low}))^2$. Note that in our estimate of the typical q, we assume that the disc semi-thickness just before downward transition is of the order of 0.15 as suggested in our numerical simulations, see Fig. 14. Following the same procedure to estimate $\sigma_{\rm rel}$ in the high state, we obtain from equation (A14)

$$\sigma_{\rm rel,max} \approx 100 B_{\rm S} M_6^{2/3} q\alpha_{-2}. \quad (45)$$

We remark that for $\alpha_{-2} > \sim 10$ as in our simulations, both $\sigma_{\rm max}$ and $\sigma_{\rm rel,\,max}$ are of the order of 1000 which, as indicated above, is favourable for misalignment.

In order to estimate values of the inclination angle, we use the results of Appendix A together with expressions (21) and (23) with $\delta = \delta_{\rm low} = 10^{-3}$, and also equations (44) and (45). Since the results of Appendix A indicate little difference between prograde and retrograde black hole rotation, we do not distinguish between these here.

Expressed in terms of variables used in this section, the quantities η and $\eta_{\rm rel}$, which measure the ratio of the alignment radius to $R_{\rm S}$ and so also characterize the disc tilt, take the form $\eta = 40 B_{\rm S}(\alpha_{-2} a M_6)^{2/3}$ and $\eta_{\rm rel} = 20 B_{\rm S} a^{2/5} M_6^{2/3}$, where we set $a = |a|$ from now on. Note that these quantities are always small for small a. From the discussion given in Appendix A, this implies that there will then always be misalignment.

Assuming that $\alpha > \alpha_{\rm crit} = 4 \times 10^{-3} a^{-2/5}$, we can use equation (A9), to obtain

$$\beta \sim \left(\frac{\sigma_{\rm max}\eta^{-3/4}}{2\sqrt{3}}\right)\beta_* \approx 0.2 B_{\rm S}^{-3/4} q\alpha_{-2}^{3/2}(aM_6)^{-1/2}\beta_*, \quad (46)$$

when the expression in parentheses is smaller than 1, with $\beta \sim \beta_*$ otherwise. The latter condition can be expressed in the form

$$\alpha_{-2} > \sim 3 B_{\rm S}^{1/2} q^{-2/3}(aM_6)^{1/3}. \quad (47)$$

When α_{-2} is smaller than 0.4, it is the relativistic correction k in equation (20), which determines the shape of the disc and we should use the results of Appendix A devoted to the case $\alpha < \alpha_{\rm crit}$. These are analogous to those of the previous case, see equation (A15), but now $\sigma_{\rm max}$ and η must be substituted by $\sigma_{\rm rel,\,max}$ and $\eta_{\rm rel}$. Using equations (A15) and (A19), we obtain

$$\beta \approx 0.2\sigma_{\rm rel,max}\eta_{\rm rel}^{-5/4}\beta_* \approx 0.5 B_{\rm S}^{-1/4} q\alpha_{-2} a^{1/2} M_6^{-1/6}\beta_*, \quad (48)$$

when $\sigma_{\rm rel,max} < 5\eta_{\rm rel}^{5/4}$, with $\beta \sim \beta_*$ otherwise. When $\sigma_{\rm rel,max} > 5\eta_{\rm rel}^{5/4}$, we have

$$\alpha_{-2} > 2 B_{\rm S}^{1/4} q^{-1} a^{1/2} M_6^{1/6}. \quad (49)$$

Equations (47) and (49) show that in order to have $\beta \sim \beta_*$ at $\tau \sim \tau_{\rm crit}$, either the viscosity parameter α should be larger than, say, 10^{-2}, or the black hole rotation parameter should be small enough. Let us stress that the fact that the inclination angle being close to that of the stream does not mean that the disc is flat. It has a twisted form as long as either $R_{\rm BP}$, in the case of $\alpha > \alpha_{\rm crit}$, or $R_{\rm rel}$ in the opposite case is larger than the size of marginally stable orbit. These conditions typically hold for accretion discs in the low state unless the rotational parameter is very small.

7 DISCUSSION

In this paper, we have considered the influence of a stream of gas acting as a source of mass for an accretion disc around a rotating black hole on the geometrical shape of the disc. Both the accretion disc and the stream are assumed to have originated from the tidal disruption of a star by the black hole. The action of the gravitomagnetic force tends to drag the disc towards the black hole equatorial plane, while the action of the stream is to cause disc material in the vicinity of the stream impact radius, $R_{\rm S}$, to align its angular momentum vector with that of the orbit the star moved in prior to disruption.

Since, in general, this orbital plane is inclined with respect to the equatorial plane of the black hole by some angle order of unity, the combined action of the stream and the gravitomagnetic force due to the black hole could result in the formation of a twisted disc. The presence of a tilted and twisted disc could have important observational consequences. In particular, it could affect the spectrum and produce variability (e.g. Dexter & Fragile 2013), produce distinctive features in emission-line profiles (e.g. Bachev 1999), provide a mechanism for the excitation of quasi-periodic oscillations through a parametric instability (e.g. Ferreira & Ogilvie 2008, 2009). In turn, measurements of disc twist and tilt could help to estimate both the black hole parameters (its mass and spin) and quantities governing the evolution of the accretion disc.

We have employed both analytic and numerical methods in our study. First, we extended the linear theory of a stationary twisted disc to incorporate an additional source of angular momentum provided by the stream in Sections 2–2.2. We used this to identify the important parameters governing the shape of the disc in Section 3.1. These were related to the ratio of the warp diffusion or propagation time to the mass accretion time and the ratio of the alignment radius to the stream impact radius. By considering both numerical solutions of the governing equation in Section 3.2 as well as an analytic approach that yielded the asymptotic dependence of the disc tilt on these quantities given in Appendix A, it was demonstrated that a large value of the first parameter and a small value of the second favoured the misalignment of a quasi-stationary disc.

We then used SPH simulations to test these results for a locally isothermal disc with aspect ratio $\sim$0.1 in Section 4. Near-disc alignment for black hole rotation parameter, $a = 1$, and significant misalignment for $a = 0.1$ were obtained for both approaches. We also found reasonable agreement for the relaxed values of the disc inclination angle, β, at the stream impact radius, $R_{\rm S}$, with a typical difference between analytic and SPH results being $\sim$30 per cent.

In order to generate more realistic models, we went on to use a one-dimensional grid-based numerical scheme to calculate the

evolution of background model discs taking into account both gas and radiation pressure in Section 5. Quantities such as the disc surface density, Σ and δ entering our equation for the disc tilt were evolved forwards in time under the assumption that the effective viscosity in the disc is described by the standard α model. The influence of the stream is taken into account through a mass source term localized in radius to the vicinity of $R_{\rm S}$. The total mass flux was set equal to that of the stream. In this way, we obtained a sequence of background models for $\alpha = 0.3$ and 0.1 without tilt, spanning times between the initial TDE and a time at which most of the disc is in a cool state. Thus, the models were evolved through a slim disc advection-dominated stage and the beginning of the transition to the radiative stage. It is important to stress that the α model predicts that this transition is accompanied by thermal instability (Shakura & Sunyaev 1976), which leads to limit cycle-like behaviour between 'high' and 'low' states of the disc with $\delta \sim 1$ and 0.001, respectively.

Using these background models, we calculated a sequence of quasi-stationary twisted disc configurations and so found the dependence of β on time in Section 5.8. We found that when the black hole rotation is close to the maximal one, $\beta \sim 0.1$ of the stream inclination, β_*, while it grows to $\sim 0.4\beta_*$ when the disc experiences transitions to low states. For smaller black hole rotations, these inclinations are larger.

With help of the asymptotic analytic theory of solutions to our twisted disc equations outlined in Appendix A, we estimate β at the low state for accretion discs with smaller values of α than those adopted above. Thus, β is found to be $\sim 0.1\beta_*$ when $\alpha \sim 0.01$ and the black hole rotation is close to maximal. The disc inclination gets smaller for smaller values of α and increases with decrease of the black hole rotation parameter.

That the disc changes its inclination during the transition to the low state could have significant observational consequences. If the orientation of the disc with respect to the line of sight is such that parts of the disc with radii of the order of $R_{\rm S}$ obscure the central source when it is in the low state, there could be intermittent dips in its luminosity. Note that such dips have indeed been observed in a candidate TDE (Liu, Li & Komossa 2014), although they have been given a different interpretation as being formed due to deflection of the stream by the gravitational field of another black hole orbiting the one that produced the TDE (Liu, Li & Chen 2009; Liu, Li & Komossa 2014). If the disc's orientation is such that both inner and outer parts of it can be observed during high and low states, the transitions could have an impact on the radiation spectrum. In particular, when parts of the disc at $R \sim R_{\rm S}$ are inclined with respect to inner ones, they can easily intercept radiation coming from the central source. Disc gas being heated up by a strong flux of X-rays could also form additional features in the radiation spectrum.

Note that a strong increase of β during a transition to the low state is expected even for disc models where the thermal instability does not operate. Unlike the models considered in this paper, in the latter case, this transition happens only once, and the subsequent alternation of β between relatively large and small values is not expected.

It is important to point out that the results of this paper should be viewed as first estimates. They have been obtained under a number of significant simplifications. Perhaps, the most crucial one would be our assumption that the disc is quasi-stationary. This holds well during the advection-dominated stage when time-scales associated with relaxation to a quasi-stationary state are shorter than the characteristic evolution time-scale of the system. However, the relaxation time-scale greatly increases during the low state. A simple estimate indicates that it is significantly longer than the evolution time when transitions between high and low states occur. Clearly, in such a situation, time-dependent calculations of the evolution of the disc tilt and twist are important. The quasi-steady disc structures we have calculated, at any time, can be viewed as targets that the system may not realize. Accordingly, the range of oscillations in β may be reduced in comparison to expectations from estimates made from quasi-stationary models. On the other hand, misalignment is expected to still remain significant.

Note too that during the advection-dominated stage, there are additional terms in the twist equation, which have been omitted, for simplicity, in this paper. One should also take into account the possibility of strong outflows during this stage from the disc. The analysis of a more complicated twist equation, which has explicit time dependence and at least partially accounts for effects determined by advection, will be the subject of a separate study.

ACKNOWLEDGEMENTS

MXG acknowledges support through Leopoldina fellowship programme (fellowship number LPDS 2009-50). Simulations were performed using the Darwin Supercomputer of the University of Cambridge High Performance Computing Service, provided by Dell Inc. using Strategic Research Infrastructure Funding from the Higher Education Funding Council for England and funding from the Science and Technology Facilities Council. MXG also acknowledges the computing time granted (NIC project number 8163) on the supercomputer JUROPA at Jülich Supercomputing Centre (JSC). PBI was supported in part by RFBR grants 15-02-08476 and 16-02-01043 and also by Grant of the President of the Russian Federation for Support of the Leading Scientific Schools NSh-6595.2016.2.

REFERENCES

Abramowicz M. A., Czerny B., Lasota J. P., Szuszkiewicz E., 1988, ApJ, 332, 646
Bachev R., 1999, A&A, 348, 71
Bardeen J. M., Petterson J. A., 1975, ApJ, 195, L65
Bogdanovic T., Eracleous M., Mahadevan S., Sigurdsson S., Laguna P., 2004, ApJ, 610, 707
Bonnerot C., Rossi E. M., Lodato G., Price D. J., 2016, MNRAS, 455, 2253
Burrows D. N. et al., 2011, Nature, 476, 421
Cannizzo J. K., Lee H. M., Goodman J., 1990, ApJ, 351, 38
Caproni A., Abraham Z., Livio M., Mosquera Cuesta H. J., 2007, MNRAS, 379, 135
Carter B., Luminet J.-P., 1983, A&A, 121, 97
Carter B., Luminet J. P., 1985, MNRAS, 212, 23
Coughlin E. R., Nixon C., Begelman M. C., Armitage P. J., Price D. J., 2016, MNRAS, 455, 3612
Demianski M., Ivanov P. B., 1997, A&A, 324, 829
Dexter J., Fragile P. C., 2013, ApJ, 730, 36
Dremova G. N., Dremov V. V., Tutukov A. V., 2014, Astron. Rep., 58, 291
Esquej P. et al., 2008, A&A, 489, 543
Evans C. R., Kochanek C. S., 1989, ApJ, 346, L13
Ferreira B. T., Ogilvie G. I., 2008, MNRAS, 386, 2297
Ferreira B. T., Ogilvie G. I., 2009, MNRAS, 392, 428
Franchini A., Lodato G., Facchini S., 2015, MNRAS, 455, 1946
Frank J., Rees M. J., 1976, MNRAS, 176, 633
Garavaglia T., 1987, Am. J. Phys., 55, 164
Guillochon J., Ramirez-Ruiz E., 2013, ApJ, 767, 25
Guillochon J., Ramirez-Ruiz E., 2015, ApJ, 809, 166
Hayasaki K., Stone N., Loeb A., 2013, MNRAS, 434, 909
Hills J. G., 1975, Nature, 254, 295
Ivanov P. B., Chernyakova M. A., 2006, A&A, 448, 843

Ivanov P. B., Illarionov A. F., 1997, MNRAS, 285, 394 (II)
Ivanov P. B., Novikov I. D., 2001, ApJ, 549, 467
Ivanov P. B., Chernyakova M. A., Novikov I. D., 2003, MNRAS, 338, 147
Ivanov P. B., Polnarev A. G., Saha P., 2005, MNRAS, 358, 1361
Ivanov P. B., Papaloizou J. C. B., Paardekooper S.-J., Polnarev A. G., 2015, A&A, 576, A29
Kelley L. Z., Tchekhovskoy A., Narayan R., 2014, MNRAS, 445, 3919
Khabibullin I., Sazonov S., Sunyaev R., 2014, MNRAS, 437, 327
Khokhlov A., Novikov I. D., Pethick C. J., 1993a, ApJ, 418, 163
Khokhlov A., Novikov I. D., Pethick C. J., 1993b, ApJ, 418, 181
Kim S. S., Park M.-G., Lee H. M., 1999, ApJ, 519, 647
Kochanek C. S., 1994, ApJ, 422, 508
Komossa S., 2015, J. High Energy Astrophys., 7, 148
Komossa S. et al., 2008, ApJ, 678, L13
Komossa S. et al., 2009, ApJ, 701, 105
Lacy J. H., Townes C. H., Hollenbach D. J., 1982, ApJ, 262, 120
Lightman A. P., Shapiro S. L., 1977, ApJ, 211, 244
Liu F. K., Li S., Chen X., 2009, ApJ, 706, L133
Liu F. K., Li S., Komossa S., 2014, ApJ, 786, 103
Lodato G., King A. R., Pringle J. E., 2009, MNRAS, 392, 332
Lubow S. H., Ogilvie G. I., Pringle J. E., 2002, MNRAS, 337, 706
Lynden-Bell D., Pringle J. E., 1974, MNRAS, 168, 603
MacLeod M., Guillochon J., Ramirez-Ruiz E., 2012, ApJ, 757, 134
Magorrian J., Tremaine S., 1999, MNRAS, 309, 447
Mainetti D., Lupi A., Campana S., Colpi M., 2016, MNRAS, 457, 2516
Miller M. C., 2015, ApJ, 805, 83
Morales Teixeira D., Fragile P. C., Zhuravlev V. V., Ivanov P. B., 2014, ApJ, 796, 103
Nealon R., Price D. J., Nixon C. J., 2015, MNRAS, 448, 1526
Paczyński B., Wiita P. J., 1980, A&A, 88, 23
Papaloizou J. C. B., Lin D. N. C., 1995, ApJ, 438, 841
Papaloizou J. C. B., Pringle J. E., 1983, MNRAS, 202, 1181
Rees M. J., 1988, Nature, 333, 523
Shakura N. I., Sunyaev R. A., 1973, A&A, 24, 337
Shakura N. I., Sunyaev R. A., 1976, MNRAS, 175, 613
Shen R.-F., Matzner C. D., 2014, ApJ, 784, 87
Springel V., 2005, MNRAS, 364, 1105
Stone N., Loeb A., 2012, Phys. Rev. Lett., 108, 061302
Stone N. C., Metzger B. D., 2016, MNRAS, 455, 859
Syer D., Ulmer A., 1999, MNRAS, 306, 35
Szuszkiewicz E., Miller J. C., 1997, MNRAS, 287, 165
Szuszkiewicz E., Miller J. C., 1998, MNRAS, 298, 888
Szuszkiewicz E., Miller J. C., 2001, MNRAS, 328, 36
Thorne K. S., Price R. H., Macdonald D. M., 1986, Black Holes: The Membrane Paradigm. Yale Univ. Press, New Haven, CT
van Velzen S., Körding E., Falcke H., 2011, MNRAS, 417, L51
Wu S.-M., Chen L., Yuan F., 2010, MNRAS, 402, 537
Zhang W., Yu W., Karas V., Dovčiak M., 2015, ApJ, 807, 89
Zhuravlev V. V., Ivanov P. B., 2011, MNRAS, 415, 2122 (ZI)
Zhuravlev V. V., Ivanov P. B., Fragile P. C., Morales Teixeira D., 2014, ApJ, 796, 104
Ziegler U., Yorke H. W., 1997, Comput. Phys. Commun., 101, 54

APPENDIX A: APPROXIMATE ANALYTIC SOLUTIONS TO THE GOVERNING EQUATION WITH ESTIMATES OF β_S FOR LARGE AND SMALL ALIGNMENT RADII

When the source term in equation (20) is set to zero and δ and ξ are constants, it can be solved exactly in two limiting cases $k \to 0$ and $k \to \infty$, see e.g. II. These cases correspond to the dominance of either viscous terms or post-Newtonian relativistic corrections in equations of motion describing the twisted disc, respectively. Its dynamics and the shape of stationary configurations differ qualitatively in these limits; in particular, as we have mentioned above when the relativistic corrections dominate and the black hole rotates in the same sense as the disc, the disc's alignment with the equatorial plane at small radii is absent.

When the source term is present, we can also find solutions in the same limits assuming that $\Delta \to 0$ in equation (12) and, accordingly δ_Δ reduces to the Dirac delta function. Then the presence of the source term in equation (20) results in a jump condition for the derivative of $\mathcal{W}$ at $r = 1$. This is easily obtained by integrating equation (20) over an infinitesimal radial domain centred on $r = 1$. Assuming that $\mathcal{W}$ is continuous, we obtain

$$\mathrm{d}\mathcal{W}_+/\mathrm{d}r - \mathrm{d}\mathcal{W}_-/\mathrm{d}r = -\sigma(1 - \mathrm{i}k)(\mathcal{W}_* - \mathcal{W}), \tag{A1}$$

where $\mathrm{d}\mathcal{W}_\pm/\mathrm{d}r$ are respectively derivatives of solutions to equation (A5) evaluated for $r > 1$ and $r < 1$ as $r \to 1$. Thus, in our analytic approach, a solution to equation (20) consists of homogeneous solutions in the inner domain ($r < 1$) and the outer domain ($r > 1$) which satisfy appropriate boundary conditions and are linked through the jump condition (A1).

A1 The case $\alpha > \alpha_{\rm crit}$

We begin by considering the case where viscous effects dominate and set $k = 0$ in equation (20). In this case, the source-free solutions can be expressed in the form

$$\mathcal{W} = z_1^{1/3}(C_1 J_{-1/3}(z_1) + C_2 J_{1/3}(z_1)),$$
$$z_1 = \frac{4}{3} c_\pm \mathrm{e}^{\mathrm{i}\pi/4} \left(\frac{\eta}{r}\right)^{3/4}, \tag{A2}$$

where $C_{1,2}$ are arbitrary constants, $J_\nu(z)$ is the Bessel functions of order ν, the $(+)$ and $(-)$ signs respectively correspond to prograde and retrograde black hole rotation, $c_+ = 1$ and $c_- = \mathrm{i}$.

The solution (A2) should satisfy two boundary conditions, $|\mathcal{W}| \to 0$ when $r \to 0$, and $\mathcal{W}' \to 0$ when $r \to \infty$, and hereafter a prime denotes the radial derivative. The inner solution, valid for $r < 1$, that satisfies the inner boundary condition can be written in the form

$$\mathcal{W}_{\rm in} = C_{\rm in}\phi_{\rm in}, \quad \text{with} \quad \phi_{\rm in} = z_1^{1/3}(J_{-1/3}(z_1) - \mathrm{e}^{-\mathrm{i}\pi/3} J_{1/3}(z_1)), \tag{A3}$$

while the outer solution valid for $r > 1$ that satisfies the outer boundary condition may be written as

$$\mathcal{W}_{\rm out} = C_{\rm out}\phi_{\rm out}, \quad \text{with} \quad \phi_{\rm out} = z_1^{1/3} J_{-1/3}(z_1). \tag{A4}$$

The jump condition (A1) can be used to find $C_{\rm in}$, $C_{\rm out}$ and accordingly, the value of $\mathcal{W}_{\rm S} = \mathcal{W}\ (r = 1)$. The calculation is straightforward with the result that

$$\mathcal{W}_{\rm S} = \frac{\sigma f \mathcal{W}_*}{\sigma f + 1}, \quad \text{where} \quad f = -\phi_{\rm in}\phi_{\rm out}/W_{\rm R},$$

with the Wronskian

$$W_{\rm R} = \phi_{\rm in}\phi'_{\rm out} - \phi_{\rm out}\phi'_{\rm in}, \tag{A5}$$

with all quantities being evaluated at $r = 1$.

With no loss of generality, we can assume that $\mathcal{W}_*$ is real and equal to β_*. Then $\beta_{\rm S}$ can be found from equation (A5) in the form

$$\beta_{\rm S} = \frac{\sigma|f|\beta_*}{\sqrt{D}}, \quad \text{where} \quad D = |f|^2\sigma^2 + (f + f^*)\sigma + 1. \tag{A6}$$

From the known properties of Bessel and Gamma functions, we obtain

$$W_{\rm R} = -\frac{2^{-2/3}3^{5/6}c_\pm^{2/3}}{\pi}\mathrm{e}^{-\mathrm{i}\pi/6}\eta^{1/2}r^{-3/2}. \tag{A7}$$

A1.1 Expressions for β_S in the limits of large and small η

Using equation (A7) together with asymptotic expressions for the Bessel functions, we can express f in equation (A5) in terms of elementary functions in the limits $\eta \gg 1$ and $\eta \ll 1$. In the former limit, we can use the asymptotic forms of the Bessel functions for large absolute values of their arguments to find

$$f = \frac{e^{i\pi/12}(1 - e^{-i\pi/3})}{2\sqrt{3}c_\pm}\eta^{-3/4}. \tag{A8}$$

When the black hole rotation is prograde, we can set $c_\pm = 1$ and obtain from equation (A8)

$$\beta_S = \frac{\sigma\eta^{-3/4}}{2\sqrt{D}}\beta_*, \quad \text{where}$$

$$D = \frac{\eta^{-3/2}}{4}\sigma^2 + \frac{\sqrt{(\sqrt{3}+2)}\eta^{-3/4}}{2}\sigma + 1. \tag{A9}$$

When $a < 0$, the expression for β_S is the same as equation (A9) with the modification that as in this case f is purely imaginary, the term proportional to σ in the expression for D is equal to zero as can easily be seen from equation (A6). Since the contribution of this term is quite small, we use equation (A9) for both prograde and retrograde rotation.

When $\eta \ll 1$, we use the asymptotic representations of Bessel function at small absolute values of their arguments to obtain

$$f = \left(\frac{2^{4/3}\pi e^{i\pi/6}}{3^{5/6}\Gamma^2(2/3)c_\pm^{2/3}}\right)\eta^{-1/2} \approx 1.17\left(\frac{e^{i\pi/6}}{c_\pm^{2/3}}\right)\eta^{-1/2}. \tag{A10}$$

Since $|f|$ is the same for both prograde and retrograde cases, for both we approximately have

$$\beta_S = \frac{1.17\sigma\eta^{-1/2}\beta_*}{\sqrt{D}},$$

$$D = 1.3689\eta^{-1}\sigma^2 + 1.17\sigma\sqrt{3\eta^{-1}} + 1. \tag{A11}$$

Taking the limit $\eta \to 0$, we obtain $\beta_S \to \beta_*$. In this case, although warp propagation is efficient, the alignment radius is arbitrarily small so that disc is unable to align with the black hole equator. As η increases, the degree of misalignment decreases, being governed by the magnitude of the quantity $\sqrt{\eta}/\sigma$. When $R_{BP} = R_S$, this is proportional to the ratio of the local accretion time-scale to the local warp diffusion time-scale. A small value of this ratio favours misalignment as expected.

On the other hand, in the opposite limit $\eta \to \infty$, corresponding to the alignment radius moving to large radii, $\beta_S \to 0$ as expected. As before, a large value of σ tends to favour misalignment.

Note that the case $\alpha > \alpha_{crit}$ and $\eta < 1$ can be realized only when the black hole mass is sufficiently small if we require that $\alpha < 1$. Indeed, from these conditions, we get $\alpha_{crit} < \alpha < (23/2)^{3/2}\delta^2(a\beta_S M_6)^{-1}$, which leads to $a < (23/2)^{5/2}\delta^2(B_S M_6)^{-5/3}$. Using again the fact that here we are considering $\alpha > \alpha_{crit} = a^{-2/5}\delta^{4/5}$, we obtain from the above condition on a that $\alpha < 2/23(B_S M_6)^{2/3}$. Since, on the other hand, α is required to be smaller than one, we must have $M_6 < \sim 39/B_S$.

A2 The case $\alpha < \alpha_{crit}$

In this case, we formally assume that the constant k in equation (20) becomes very large. In this limit, the homogeneous solutions to equation (20) can be written as

$$\mathcal{W} = z_2^{3/5}(C_1 J_{-3/5}(z_2) + C_2 J_{3/5}(z_2)), \quad \text{where}$$

$$z_2 = \frac{2\sqrt{3}}{5c_\pm}\left(\frac{\eta_{rel}}{r}\right)^{5/4}, \tag{A12}$$

and we recall that η_{rel} is given by equation (23). As for the previous case we introduce inner and outer solutions according to the specification

$$\mathcal{W}(r < 1) = C_{in}\phi_{in}, \quad \text{and} \quad \mathcal{W}(r > 1) = C_{out}\phi_{out}, \tag{A13}$$

where ϕ_{in} and ϕ_{out} are proportional to combinations of Bessel functions discussed below. The expression (A5) is modified by the substitution $\sigma \to -ik\sigma$:

$$\mathcal{W}_S = \frac{i\sigma_{rel} f \mathcal{W}_*}{i\sigma_{rel} f + 1},$$

$$\sigma_{rel} = k\sigma = \frac{12\lambda GM}{\delta^2 c^2 R_S}\left(\frac{\dot{M}_S}{2\pi\Sigma R_S^2}\sqrt{\frac{R_S^3}{GM}}\right). \tag{A14}$$

As we will see below that now f is real and positive in both limits of large and small η_{rel}. Using this fact, we easily obtain from equation (A14) that

$$\beta_S = \frac{f\sigma_{rel}}{\sqrt{f^2\sigma_{rel}^2 + 1}}\beta_*. \tag{A15}$$

Note that σ_{rel} plays the role of σ in this case and may be regarded as being equal to σ with α set equal to $3\lambda GM/(c^2 R_S^2)$.

As we have discussed above, when $\alpha < \alpha_{crit}$, there is a qualitative difference in behaviour of solutions of the governing corresponding to different signs of a (see Section 3). Therefore, it is convenient to treat them separately.

A2.1 The case of prograde rotation $a > 0$

We recall that when $a > 0$, z_2 is real and the inner oscillating solution is characterized by a phase, Ψ, which is determined by conditions close to the last stable orbit, where one must consider a fully relativistic theory of twisted discs, see ZI for such an approach. Here we shall fix this phase, Ψ, to be equal to $-2\pi/3$, which is obtained in a certain limit discussed in ZI. In order to comply with the notation of this paper, we write the inner solution in the form

$$\phi_{in} = z_2^{3/5}\left(\cos(\Psi - \pi/20)J_{-3/5}(z_2) + \sin(\Psi + \pi/20)J_{3/5}(z_2)\right) \tag{A16}$$

while the outer solution is given by $\phi_{out} = z_2^{3/5}J_{-3/5}(z_2)$. The Wronskian W_R of this pair can be written as

$$W_R = (54/5)^{1/5}\pi^{-1}\sin(2\pi/5)\sin(\Psi + \pi/20)\eta_{rel}^{3/2}r^{-5/2}. \tag{A17}$$

When $\eta_{rel} \gg 1$, we approximately have

$$f = \frac{2}{\sqrt{3}}\frac{\cos(z_S - \Psi)\cos(z_S + \pi/20)}{\sin(\Psi + \pi/20)}\eta_{rel}^{-5/4}, \tag{A18}$$

where $z_S = z_2(r = 1) = 2\sqrt{3}/5\eta_{rel}^{5/4}$.

In order to obtain an order-of-magnitude estimate of β_S, we further simplify equation (A18) by averaging over z_S to obtain

$$f = \frac{1}{\sqrt{3}}\tan^{-1}(\Psi + \pi/20)\eta_{rel}^{-5/4} \approx 0.22\eta_{rel}^{-5/4}, \tag{A19}$$

where we assume $\Psi = -2\pi/3$ to obtain the last equality.

In the opposite limit $\eta_{\rm rel} \ll 1$, we get

$$f = (5/27)^{1/5} \left(\frac{2\pi}{\Gamma^2(2/5)}\right) \left(\frac{\cos(\Psi - \pi/20)}{\cos(\pi/10)\sin(\Psi + \pi/20)}\right) \eta_{\rm rel}^{-3/2} \approx 0.645 \eta_{\rm rel}^{-3/2}, \quad \text{(A20)}$$

where we have again set $\Psi = -2\pi/3$ in the last equality.

As expected, when the alignment radius approaches zero with $\eta_{\rm rel} \to 0$, we obtain $\beta_{\rm S} \to \beta_*$ corresponding to complete misalignment. Similarly in the opposite limit with $\eta_{\rm rel} \to \infty$, we obtain $\beta_{\rm S} \to 0$, corresponding to complete alignment. The magnitude of the quantity $\sigma_{\rm rel}$ then determines the degree of misalignment for a given $\eta_{\rm rel}$ through equation (A15), with a large value favouring misalignment.

A2.2 The case of retrograde rotation $a < 0$

When $a < 0$, z_2 is purely imaginary and the inner solution is fixed by the requirement that the disc inclination should tend to zero at small r. We then have

$$\phi_{\rm in} = z_2^{3/5}(J_{-3/5}(z_2) - {\rm e}^{-{\rm i}3\pi/5} J_{3/5}(z_2)), \quad \text{and}$$

$$\phi_{\rm out} = z_2^{3/5} J_{-3/5}(z_2), \quad \text{(A21)}$$

which lead to

$$W_{\rm R} = -(54/5)^{1/5}\pi^{-1}\cos(\pi/10)\eta_{\rm rel}^{3/2} r^{-5/2}. \quad \text{(A22)}$$

When $\eta_{\rm rel} \gg 1$, we find from equation (A5) that

$$f = \frac{1}{\sqrt{3}} \eta_{\rm rel}^{-5/4} \approx 0.58 \eta_{\rm rel}^{-5/4}, \quad \text{(A23)}$$

and when $\eta_{\rm rel} \ll 1$ we obtain

$$f = 2\pi(5/27)^{1/5} \left(\cos(\pi/10)\Gamma^2(2/5)\right)^{-1} \eta_{\rm rel}^{-3/2} \approx 0.96 \eta_{\rm rel}^{-3/2}. \quad \text{(A24)}$$

From equation (A15) and the expressions (A23) and (A24), it follows that the estimate of $\beta_{\rm S}$ for the retrograde case will be to order of magnitude the same as for the prograde case.

This paper has been typeset from a TEX/LATEX file prepared by the author.